

***Innate defensive behavior in response to visual stimuli in awake and head fixed mice.***

---

**Simon E. Lansbergen**

Master student, Medical Natural Sciences VU-University.

# ***Innate defensive behavior in response to visual stimuli in awake and head fixed mice.***

---

## **Abstract**

Investigating the extent of fear a mouse experiences when a threatening looming stimulus is presented, could provide insight in the working of the neural circuitry of innate responses and behaviors. Innate defensive behavior causes freezing behavior in mice which lead to differences in physical state intended for surviving dangerous situations. Observations and analysis of these responses can be utilized in explaining and understanding human emotion and behavior. We designed an experiment setup, as well as methodology and recorded mostly: muscle activity, pupil size and pupil movement activity. Optical imaging intended for (wide field) calcium imaging was included for future experiments. We investigated two types of stimuli, a strong light reflex and a threatening looming disc type. The first experiment produced as expected a significant ( $p < 0.001$  &  $p < 0.01$ ) decrease and increase in mean pupil size and activity before and after the stimulus, providing essential information for the design of new and improved stimuli (e.g. minimum inter-stimulus time). A second experiment (looming disc) showed significant ( $p < 0.05$  &  $p < 0.01$ ) differences between mean EMG activity before and after the stimulus. More important differences were found between the mean pupil size and mean pupil activity, which could become statistically significant within an acceptable amount of trials ( $n=50$ ). Our results provided useful and relevant details about EMG, pupil size and movement activity and suggests that there is a stimulus effect detectable in the physical state of the mouse. In conclusion, our findings matched our goals regarding the expected experiment results and will contribute to more advantageously results in future research.

Author: Simon E. Lansbergen, BAsC.

Master student, Medical Natural Sciences, track Medical Physics. VU University Amsterdam.

Student number: 2537839.

Date of submission: 8-7-2016.

This thesis is part of a major research project in a joint collaboration between the VU University/VU Medical Centre and the Netherlands Institute for Neuroscience (NIN).

1<sup>st</sup> Supervisor: dr. J.A. Heimel (NIN)



2<sup>nd</sup> Supervisor: dr. B.W. van Dijk (VUmc)



Contact details lead assessor:

Dr. J. A. Heimel  
Meibergdreef 47  
1105 BA Amsterdam  
Tel.: 020 5665500  
E-mail: heimel@nin.knaw.nl

Student:

S.E. Lansbergen  
Baden Powellweg 77, 1069 Amsterdam  
E-mail: simon.lansbergen@gmail.com

# Index

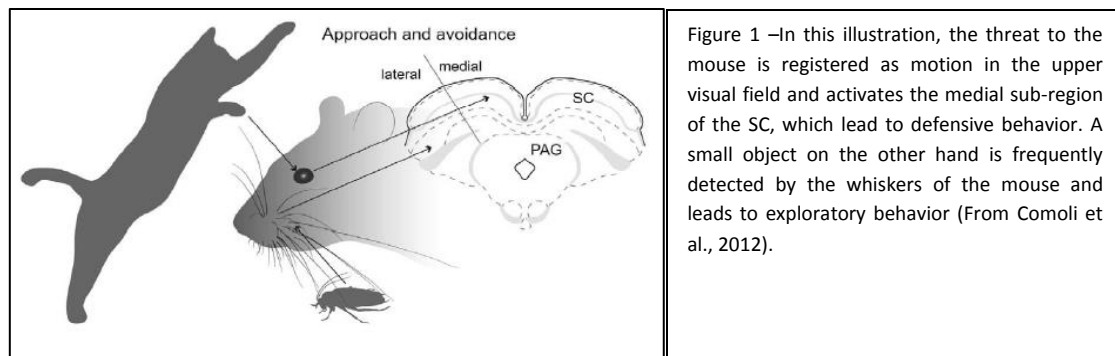
Abstract .....	2
Introduction.....	5
Methods .....	7
1. Animals .....	7
1a. Head fixed and chronic imaging window preparation .....	7
1b. Custom head fixation post and restraining body .....	8
1c. Mouse handling and training .....	8
2. Behavioral experiment setup and visual stimuli .....	9
2a. Visual stimuli.....	10
2b. Heart and Breath rate .....	11
2c. Electromyography (EMG) .....	12
2d. Ultrasonic sound recording .....	13
2e. Pupil size recording.....	14
2f. Optical Imaging: wide-field calcium imaging .....	17
3. Data analyses.....	19
3a. Heart and Breath rate.....	19
3b. EMG .....	21
3c. Ultrasound .....	22
3d. Pupil recording analysis.....	23
Results .....	25
1. Validation experiment.....	25
2. Looming disc measurement .....	29
2a. Individual trial result.....	29
2b. Session results .....	31
Discussion .....	35
References.....	39
Appendix.....	42

## Introduction

Human emotion and behavior is a popular topic in research and a vast amount of papers have been published regarding this topic in many fields, including neuroscience. Although, there are certainly exclusive characteristics of human emotion and behavior, there are some features that are shared by both human and animal through a common ancestor (LeDoux, 2012). Emotions such as fear and anxiety have similar underlying neural circuitry in other species, including rodents, compared to that found in humans (Sokolowski and Corbin, 2012). When exposed to a threat, like an approaching predator, rodents often show an unconditioned defensive response. The latter is usually referred to as innate behavior and can be formulated as behavior that requires no prior learning. Innate behavior is particularly rigid and predictable, it usually involves basic life functions (LeDoux, 2012) like responses to fear. The well-known fight-or-flight response is an extreme sympathetic response elicited by fear that every animal or human possesses (Kandel, 2013). These unconditioned responses to fear are driven by ancient, but still well conserved neural circuitry (Wei et al., 2015; Sokolowski and Corbin, 2012). Regardless of the fact that unconditioned fear response to different threat stimuli varies between different species, there are basal underlying components in the fight-or-flight response shared by both human and animal (LeDoux, 2012). This shared relation is now used in human anxiety disorders studies (e.g. phobias), since similar changes in physiological indicators and behavioral responses to fear and painful stimuli, seem to be shared among humans and animals (Buccafusco, 2009). That is why knowledge and understanding of innate behavior in animals is of great value when unraveling neural circuitry and mechanisms in the brain concerning sensory input and brain state (LeDoux, 2012). Moreover, knowledge derived from studies aimed at understanding the function of innate behavior in animals, can be used in understanding human emotion and behavior (Sokolowski and Corbin, 2012; Buccafusco, 2009).

In addition to the defensive flight response, fear induced by an approaching aerial predator can also evoke (defensive) freezing behavior in mice and other (nocturnal) rodents (Liang et al., 2015). Such an event can successfully be imitated by looming stimuli, like a shadow approaching from above or an expanding disc (Wei et al., 2015; Liang et al., 2015; Yilmaz and Meister, 2015), or by models such as the classical hawk/goose model used by Tinbergen and Lorenz in their famous 1937 experiments (Schleidt and Shalter, 2011). Freezing is known to affect various motor responses, as well as hormone control and the autonomic nervous system (ANS) (Comoli et al., 2012; Kandel, 2013). The sudden flood of hormones released in a freezing situation results in a change of the physical state of the mouse, intended for surviving dangerous situations (LeDoux, 2012). Known functions to be affected by the ANS in mice are for instance, heart rate (bradycardia), respiratory rate and pupil response (dilation and constriction). Changes in these physical states can reveal the extent of the innate defensive fear responses a mouse shows to different threatening stimuli.

Not only has the mouse become important in behavioural research, it has also emerged as a powerful model system for studying vision, since most, though not all, basic properties of visual function are present in the mouse (Niell, 2011). Furthermore, mice are often used in research for their versatility and ease of application. Previous research indicate that mice are especially susceptible to show freezing behavior when looming stimuli are presented in the upper visual field (Shang et al., 2015; Comoli et al., 2012). The size of the mouse and its habitat are the primary reason why predators are most frequently discovered as motion in the upper visual field (Fig. 1) (Comoli et al., 2012). The information from the upper visual field is processed by the primary visual cortex (V1) and secondary visual cortices, which have a distinct spatial organization known as a retinotopic map (Niell, 2011). The primary visual cortex projects massively on the superficial layers of the superior colliculus (SC), which is an important mid-brain structure that is involved with the production of innate defensive behaviour and is related to motor functions (Liang et al., 2015; Comoli et al., 2012). Additionally, the secondary visual cortices projects to both the intermediate and deep layers of SC. Recently, evidence has been found that the visual cortices directly contribute to freezing behavior, which include modulating the SC (Liang et al., 2015).



Many authors describe the use of freely moving mice and other rodents for the purpose of studying and analyzing freezing responses. One of the main issues concerning such studies is that as a mouse can roam freely their perceptive environment changes constantly, resulting in a relative shift of the stimulus on the retinotopic map of the mouse. This makes it very hard to apply a controlled stimulus, since the mouse can move its head freely and no control over the position of the stimulus on the retinotopic map can be acquired. Furthermore, extracting physiological data like heart rate, muscle activity and pupil dilation and constriction proves to be very difficult and induces more stress in the animal, since more invasive techniques need to be used (Whelan, 2003). On the other hand, when a mouse is in a constrained or sedated (anesthetized) situation, freezing response cannot simply be registered by the lack of movement.

The aim of this research project was to design an experiment setup with capabilities to capture brain activity and physiological change, as a function of innate defensive behavior in response to different types of (threatening) looming stimuli. Furthermore, preliminary data acquired with this newly built setup was used to further optimize the experiment setup, as well as in the design of more optimal stimuli. These stimuli consist of a variety of predator like models such as used by Tinbergen and Lorenz (Schleidt and Shalter, 2011), but also expanding disc like stimuli and light reflex (light on/off) stimuli, which served as baseline data. For future brain activity measurements, we added the possibility of wide field calcium imaging (WFCI) to the setup. Calcium imaging is a commonly used technique for investigating the areas of the visual cortex *in vivo*. To overcome the problem of the ever changing environments of freely moving mice, we head fixed the mice. This resolves the poor control over the presented stimuli and made implementation of WFCI possible, as the stimulus could now be controlled with respect to its projection on the retinotopic map of the visual system. The brain activity of our interest comes from these visual brain areas, in particular the primary and secondary visual cortex, as well as the SC. Since freezing behavior is not easy to detect when the head of the mouse is fixated, we additionally investigated four types of physical responses: 1. heart and respiration rate, as these are known to change in response to the presence of real predators (Wei et al., 2015). 2. muscle activity as measured by electromyography (EMG) recordings, freezing behavior is reflected in a decrease of muscle activity (Steenland et al., 2012). 3. pupil size and movement, as pupil size is known to correlate with attentional state (Kandel, 2013). 4. alarm calls, as rodents are known to evoke alarm calls, especially in the presence of other rodents (Grimsley et al., 2016; Wöhr and Schwarting, 2013). Thereby, investigating the extent of fear the mouse experiences when a variety of threatening looming stimuli are presented, proving insight in the working of the neural circuitry related to innate responses and behaviors, which can be utilized in explaining and understanding human emotion and behavior.

# Methods

## 1. Animals

In this study we used two different strains of mice, a transgenic strain of mouse for the behavioral experiments and three older (retired) lab mice to validate the experiment (setup/methodology) on. For the behavioral experiments a transgenic male mouse (type: Thy1-GCaMP6f) aged 8+ weeks was used, which features GCaMP6 expression in the entire brain including the visual cortices and the SC. This mouse was surgically prepared to be in head fixated position. Before we began our behavioral experimenting we tested different parts of the setup on three older lab mice, two males and one female. When not experimenting, the mice were kept in an environment with a fixed normal day and night cycle (daytime: 7:00-19:00), and room temperature (21 deg. Celsius). All experimental procedures used in this study were already approved and are part of an on-going PhD project. The original design of that study was submitted to and approved by the Committee on Animal Experimentation (in Dutch this is the '*Dieren Experimentencommissie*' or '*DEC*') of The Royal Netherlands Academy of Arts and Sciences (DEC-KNAW). Additionally, an addendum was written to facilitate the current research aim.

### 1a. Head fixed and chronic imaging window preparation

All surgical procedures were performed by a trained and experienced PhD-student from Heimel lab (part of the Netherlands Institute of Neuroscience). The window used for chronic imaging has a diameter of 0.9 mm and is made from glue substance and clear dental cement (on top of the skull), and was placed directly underneath the fixation ring. This glue was added to encapsulate water and to prevent the skull from drying out, dental cement provides a hard protection layer. The fixation ring (Fig. 2) has a handlebar on both side, which fits seemingly in the rig built for the experiment.



Figure 2 – Photo taking during surgery: the mouse is under isoflurane anesthesia. The skull is removed and a chronic imaging window prostheses with a metal ring on top to is fixed to the head. Afterwards the mouse went in recovery for 7+ days, before any experiment took place.

### 1b. Custom head fixation post and restraining body

Custom build equipment was used for the purpose of restraining and fixing the mouse into a solid position, while maintaining room for the mouse to move. To restrain the mouse we used a plastic, semi-tube like object with a solid base with a movable cover. The restrainer used in this study is shown in the upper left picture of figure 3. The inside of the semi-tubular object is coated with a conductive foil, which was connected to the ground-input of the differential amplifier used for the heart rate and muscle activity recordings. The ring on the head of the mouse was clamped between the two poles of the fixation post (bottom picture left). The combination of both did required a height adjustable platform. Between the restrainer and the ring on the head is room for the heart rate sensor.

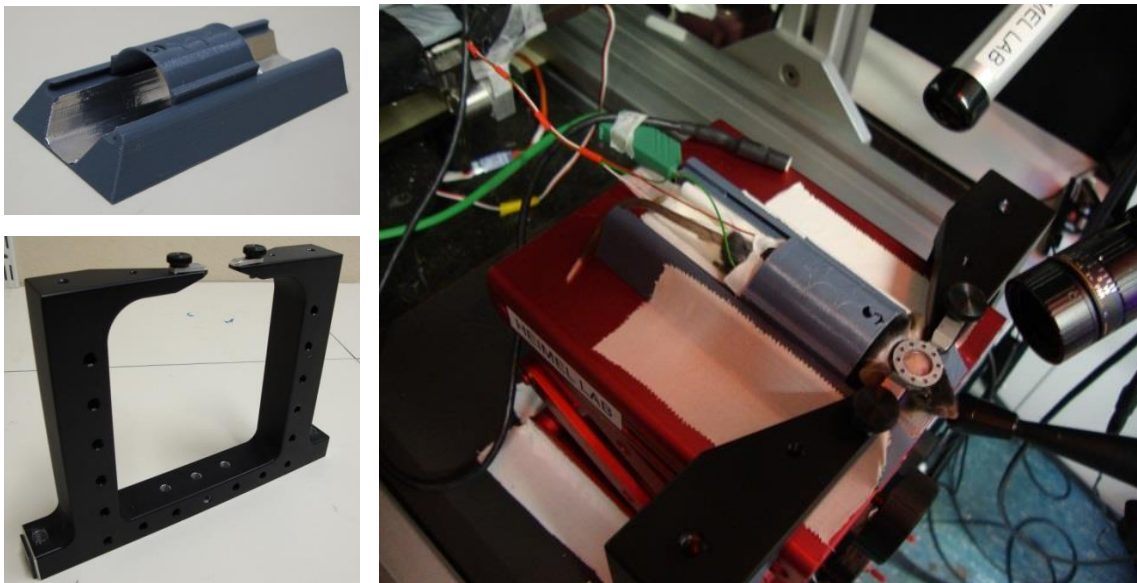


Figure 3 – Parts of the experiment setup. Picture top left: a custom build (printed) restrainer, coated with a conductive foil for grounding. Picture bottom left: head-fixation post, the ring of the mouse clamped between the tapered bars of the post. Picture right: The combination, the restrainer is fixed to the elevated platform such that ring on the head can be fixed. A camera is also attached to the post.

### 1c. Mouse handling and training

The mouse is both restrained and head fixed and this naturally induces stress in the animal (Grimsley et al., 2016). To make the mouse as comfortable as possible, it is trained to sit in a restrained and head fixed situation for about one hour. At least a week before starting the experiments, the mouse was trained and handled daily to be in the restrained and head-fixed position for increasing time spans. Eventually the mouse settles to the fixed position and natural grooming behavior is observed after some time. After experimenting the mouse got a small reward, when back in its cage.



## 2. Behavioral experiment setup and visual stimuli

For this experiment, four types of physical responses related to innate defensive behavior were recorded: heart and respiration rate, muscle activity, pupil size, and alarm calls. Furthermore, brain activity from the visual brain areas, and the SC was recorded. Also, respiration rate was derived by analysis of the raw heart rate signal. The experiment setup (Fig. 4), was designed to meet the specific needs of such recordings. The complete setup consists of several interacting components:

- Multiple acquisition systems (i.e. slave systems) for different types of physical responses.
- An optical imaging macroscope for brain activity.
- A screen driven by a stimulus-PC for presenting stimuli.
- A system that drives the acquisition and stimulus systems (i.e. master system).

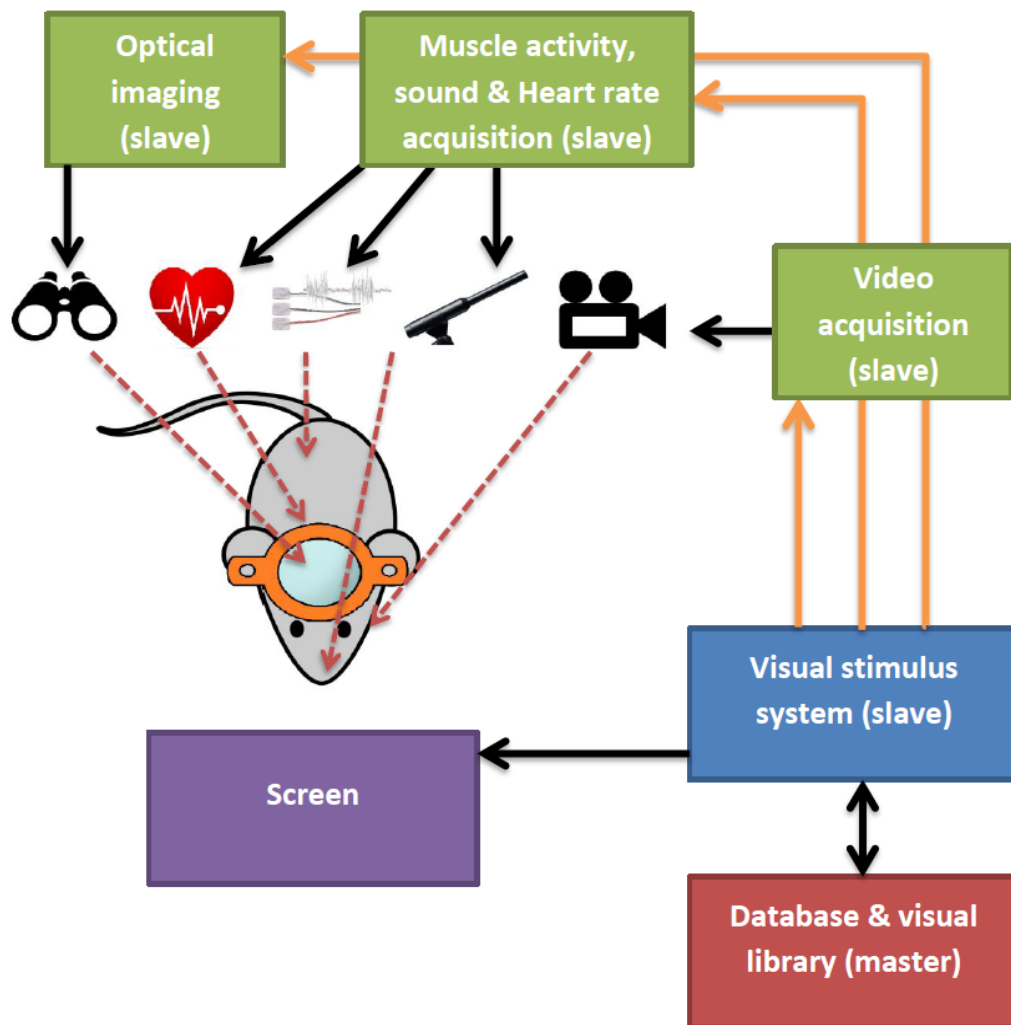


Figure 4 – Experiment setup. The green blocks represent the three acquisition system used in our experiment. The optical imaging system drives the macroscope hardware and stores collected data together with software settings (e.g. ROI and frame rate). The second acquisition system records both heart rate, muscle activity and sound. Heart rate and muscle activity are recorded using shared acquisition hardware, all recordings were stored together with relevant acquisition parameters. The last acquisition system is responsible for pupil measurements, via a real-time video stream and analysis. Acquisition was synchronized by the visual stimulus system (blue block), which also parsed trial duration and save location into the various acquisition systems. Besides synchronization, the visual stimulus system presented pre-loaded stimuli to the mouse via a screen (purple block). The experiment and visual stimuli database were located on the master system (red block). The master system was used to initiate different trial as it drives the visual system, which starts synchronized acquisition.

Synchronization and communication between different parts of the experiment setup is either done by TTL-based synchronization (initiated by the master system) or by writing a file on a remote or local network location (communication between systems). The latter is mandatory to provide the (slave) systems with trial parameters, such as duration and save location of the acquired data, whereas TTL-synchronization is used to sync acquisition between the multiple acquisition systems. Apart from the acquisition systems we used an oscilloscope (Tektronic, TDS2001C) to monitor incoming muscle activity (or heart rate) during the behavioral experiments, as muscle activity measurements did not provide in real-time monitoring of the raw muscle activity signal.

The optical imaging acquisition system, visual stimulus system and master system were already present at the Heimel Lab. For this study we added the two additional systems for the acquisition of heart rate, respiration rate, muscle activity, sound and pupil size. Software was mainly written on X32 and X64 Matlab versions on Windows 7 X64, to fit into to existing lab setup.

## 2a. Visual stimuli

Visual stimuli for these experiments can be divided into two types of visual stimuli: looming type stimuli and moving predator like type stimuli. Both types of stimuli are known to evoke innate defensive behavior (Schleidt and Shalter, 2011). The strongest freezing reactions are often obtained using a (repetitive) looming disc in an overhead position (Fig 5) with clear dark edges in contrast to the background (Yilmaz and Meister, 2013). Alternatively, a model of an aerial predator is often used, entering and moving from side to side in a straight line on the monitor, again with clear dark edges in contrast to the background.

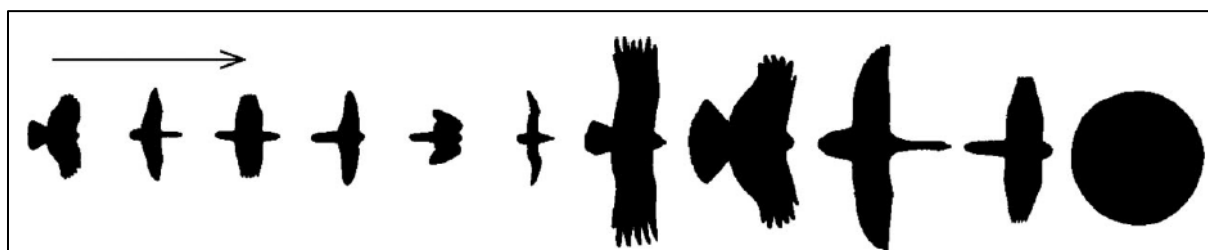


Figure 5 – This picture was taken from a paper by Schleidt and Shalter (2011), and shows several predator and non-predator aerial silhouettes. The arrow indicates the direction of the stimulus, except for the last stimulus. This dot is used in a positional static, but looming fashion.

This research project uses a looming dot stimulus in an overhead position to elicit innate defensive behavior. One of the main goals of this project is to reveal baseline information on the (physical and neurological) reaction of the mouse to strongly fear evoking stimuli. The used stimulus was a circular shaped figure (disc) with diameter, which expanded from 0 to 500 pixels in 0.25 seconds in the center of the screen, and stayed fully expanded for another 0.25 seconds. This was repeated 15 times, yielding a total stimulus time of 7.5 seconds. For further analysis of (baseline) results, 3 seconds of pre-time and 20 seconds of post-time were introduced to the final stimulus script (to capture a possible increase or decrease in physical and neural activity). The background of the disc was set at 50% gray value intensity, the disc itself set at 100%. Another stimulus type we used was an on/off stimulus. This is a stimulus in which the monitor jumps instantly from 100% black to 100% white.

The stimuli were displayed on a 23 inch LCD monitor (from Dell, type: U2312HMT), having a resolution of 1920x1080 pixels. The stimulus monitor, driven by the stimulus-PC, was placed directly over the head of the mouse and next to optical imaging setup. The area around the monitor and mouse was darkened by a light blocking curtain to limit unwanted visual distraction and so misinterpreted response by the mouse. The stimuli were programmed in MatLab using PshychToolbox 3.0 and stored on the master system. PshychToolbox 3.0 is a toolbox designed for vision and neuroscience research that provides the researcher with precise control over

visual stimuli. Before each measuring session the stimulus data was parsed into the stimulus-PC, which then awaited a TTL-pulse from the same master system before presenting the stimulus. Via this TTL-communication all acquisition (/slave) systems are also activated. Prior to each trial of each recording session, stimulus parameters were stored besides the acquisition data. Information, such as stimulus duration and trial duration were later used in the analyses of the individual trials.

## 2b. Heart and Breath rate

Both heart and breath rate are an important physical measure in the detection of fear related behavior (Meijer et al., 2005). An increase or decrease of these rates, is driven by the ANS and initiated by a change in brain state, like acute stress (Meijer et al., 2005). The normal heart rate in mice ranges between 500 and 700 beats per minute in rest, but can reach peaks up to 800-900 beats per minute in stressful situations (Ho et al., 2011). For heart and breath rate recordings in the awake mouse we used a pulse-oximeter (type: MouseOx Plus) from Starr Life Sciences Corp, fitted with a supplementary sensor. Pulse-oximetry is a non-invasive and generally accepted method for monitoring mammalian heart rate, breath rate and blood oxygen saturation (Ho et al., 2011). With this method, oxygen saturation is probed by making use of the absorption differences of red and infrared light between deoxy- and oxyhemoglobin (Boron & Boulpaep, 2012).

The pulse oximeter has a sensor, which is basically a large clip or clamp and must be placed over clear tissue with an arterial vessel present between the ends of the sensor. The clip holds a photosensitive sensor and two narrowband light sources, emitting light with different wavelengths (red and infrared). This light is partially absorbed by tissue and blood, as deoxy- and oxyhemoglobin have different absorption characteristics for both red and infrared light (Fig. 6). While light passes through tissue and blood, absorption is measured by the photosensitive sensor on the other end of the clip. The pulse oximeter computes the ratio between deoxy- and oxyhemoglobin, by comparing differences in absorbed red and infrared light. Because signal strength varies with the filling of the arteries, the pulse oximeter can also calculate the frequency of the heartbeat. The expansion of the arterial vessel correlates well with the heart beat and breath rate (Boron & Boulpaep, 2012), our primary interest.

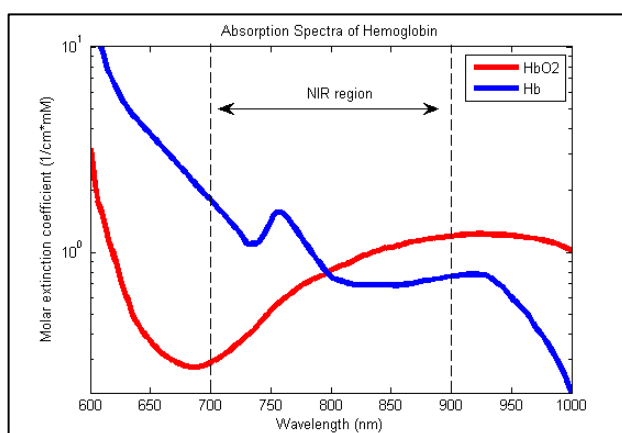


Figure 6 – light absorption characteristics of oxygenated (red curve) blood (HbO<sub>2</sub>) and de-oxygenated (blue curve) blood (Hb). In this graph molar extinction coefficient is plotted against wavelength of electro-magnetic radiation (i.e. light). The pulse oximeter computes the ratio of absorbed red and infrared light, which are separated approximately by 200 nm (oximetry.org, 2016).

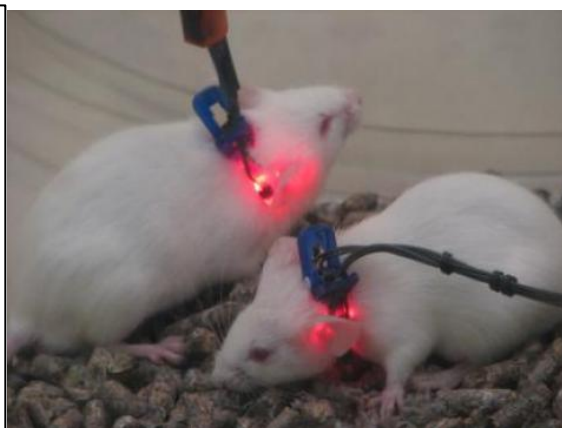


Figure 7 - Example the of the pulse-oximeter collar sensor in awake mice. (starrlifesciences.com, 2016)

In our experiment we used a collar sensor (Fig. 7), this type of sensor requires the removal of all hair at the place where the ends of the clip are placed. This can be done either by trimming the hair or chemically

removing the hair with a hair removal product. We found that trimming the hair with a small battery operated shaving device, gave the best heart rate results and was the most convenient for the mouse.

The raw signal from the pulse-oximeter was recorded and stored with Matlab and used in offline analysis of heart and breath rate. The pulse oximeter was equipped with an USB 2.0 output for direct connection to a pc, but had also an output for raw heart rate signal. The acquisition system that captured the raw signal was equipped with a 12-bit data acquisition board (DAQ) from Measurement Computing (type: PCI-DAS6025), set at a sampling rate of 5 kHz. This important parameter was chosen carefully, since the acquisition system that was used for the heart and breath rate recordings, was also used for the recording of muscle activity. The raw signal from the pulse oximeter was not additionally amplified nor was it filtered before acquisition by the DAQ. During experiments we used software supplied by the manufacturer (Standard Starr Pulse Oximeter software package, ver. 1.4), which includes basic real-time monitoring of heart and breath rate (recording the signal was not available in basic monitoring software). This software used the onboard DAQ and USB 2.0 interface in the pulse oximeter device to retrieve heart rate and oxygenation information.

The heart and breath rate acquisition system communicates with the stimulus system, which sets the duration of the experiment trail and location of the trial data. When this data is parsed into the acquisition system, it waits for a TTL-pulse to be detected by the DAQ. When all other acquisition (slave) systems are set, a final acquisition trigger is given and acquisition of the raw heart rate signal starts immediately. When acquisition is finished, the acquisition system will again await new trial information, containing trial duration and data location. Software used for acquisition of heart and breath rate, the setup of the DAQ and automatically storage of data, were written MatLab (using Matlab's data acquisition toolbox).

## **2c. Electromyography (EMG)**

When muscles are used they produce electrical currents (Whelan, 2003), that can be evaluated and recorded. Basically, electromyography or EMG records the electrical activity originating within muscles (Whittaker, 2011). When a mouse freezes for a brief period of time, the complete absence of bodily movement (with exception for breathing) is reflected by a decrease of 'signal' on the EMG results (Steenland et al., 2012, Steenland and Zhuo, 2008). That is why EMG are used to investigate the physical response to a threatening situation, such as overhead looming stimuli.

There are several methods to obtain EMG recordings, which mainly differ in the type of electrode used (Whittaker, 2011; Scholle et al., 2005; Ives and Wigglesworth, 2003; Whelan, 2003). Surface electrodes are an accepted tool in the evaluation of muscle activity in kinesiological studies (Ives and Wigglesworth, 2003). Surface EMG or sEMG was used as a non-invasive alternative to needle electrodes, as these introduce an extra surgery and additional care and handling of the animal. In this study we made use of small surface cup-electrodes (Fig. 8), which were 4 mm in diameter and made from silver/silver-chloride (Ag/AgCL). When cup-electrodes were used, the site of the cup-electrodes on the mouse must be shaven fairly clean, to improve conductivity with the skin and the underlying muscle. Conductive gel (*Signa gel*) was applied to the electrode to conduct electrical activity, and the electrodes were fixed (prior to the experiment, awake) with regular sports tape (*Hansaplast stevige sporttape*) to the skin of the mouse. The fixation of the electrodes ensures a sound connection throughout the recording session when the animal is awake, but restrained. Simple, adhesive disposable electrodes, which we customized to fit the hind leg of a mouse, proved to be inadequate in terms of noise constrains and durable fixation.

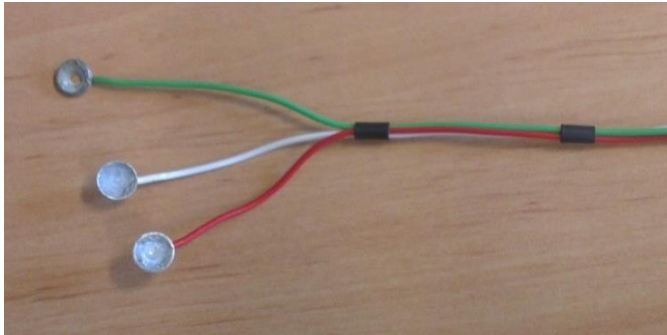


Figure 8 – Small and flexible, silver/silver-chloride (Ag/AgCl) cup-electrodes were used for EMG recordings and placed on the hind limb of the mouse leg. The electrodes were filled with a conductive gel and fixed with adhesive tape to the skin of the mouse.

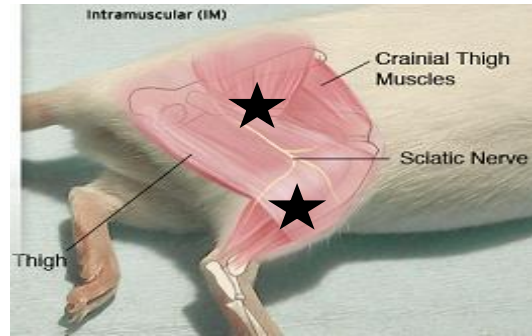


Figure 9 – The muscle anatomy of the hind limb of a mouse on top of a picture of a hind limb ([www.theodora.com](http://www.theodora.com), 2016). The black stars indicate the site were we positioned the cup-electrodes. The third (active grounding) lead was placed the on the back of the mouse, with adequate distance from the active electrodes. The electrode site was merely shaven and prepped prior to the experiments.

The cup-electrodes were positioned on the hind leg of the animal, as illustrated in figure 9. To safeguard the signal from external noise sources, a third cup-electrode was used, which was attached to a driven shield from the differential amplifier (Rich, 1983). For optimal results the electrodes were re-chlorided when the surface of the electrode became less dark (by losing the Ag/AgCl layer). This was done by means of electrolysis of the electrodes in a 5% Sodium Chloride (NaCl) water solution. For our EMG recordings we used a differential amplifier from A-M Systems, model 1700, with four separate differential channels. Each channel can be set for 100X, 1000X or 10000X amplification with variable high-pass and low-pass settings. To digitalize the signal from the amplifier, we used the same data acquisition board that was also used in the heart and breath rate recordings. The acquisition parameters for analogue to digital conversion are likewise identical to those in the heart and breath rate recordings, since both recordings share the same acquisition system. The sampling rate of the data acquisition was chosen to accommodate both heart and breath rate recordings, as well as EMG recordings. The latter has the highest temporal frequency component, and dictates the final sampling rate. As oversampling of EMG signal has no negative effect on the analysis of the digitized EMG signal (Ives and Wiggelsworth, 2003), we see no evidence that this would negatively affect either heart or breath rate analysis. Thus, for the acquisition of the EMG we use a sampling rate of 5 kHz, which is a common (Steenland et al., 2012; Scholle et al., 2005) and had ample resolution (Ives and Wiggelsworth, 2003) to capture both heart and breath rate, as well as muscle activity.

According to work by Ives and Wiggelsworth (2003) the highest frequency components of sEMG reported are around 500 Hz. High- and low-pass filter settings could be set manually on the amplifier, which made the need for comprehensive filtering afterwards unnecessary. The bandpass filter was set at 100 Hz (high-pass) and 1000 Hz (low-pass). Total gain was set at 10000X, which amplified the original signal into the range of several millivolts to volts. When the signal was amplified and digitized it was further processed and analyzed in custom written MatLab scripts.

## 2d. Ultrasonic sound recording

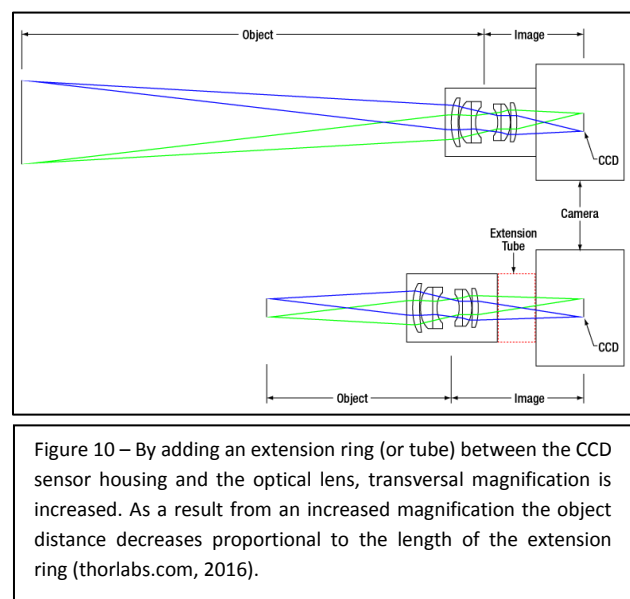
Mice are known to vocalize in many different frequency ranges, audible and far beyond the audible capabilities of humans i.e. ultrasonic (Portfors, 2006). The vocalizations that mice produce can be divided into three categories: ultrasonic vocalization (USV), low frequency harmonics (LFH) vocalizations and 'noisy' vocalizations (Grimsley et al., 2016). The power spectrum of the USV's lies completely above 20 kHz (the absolute temporal threshold of the human ear) (Wohr and Schwarting, 2013), whereas LFH vocalizations have harmonics near 5 kHz and up to 100 kHz (Grimsley et al., 2016). It is known that rodents vocalize when fear is evoked (Wohr and

Schwartz, 2013), and recent studies show that LFH vocalization may reflect the level of anxiety in mice (Grimsley et al., 2016). Mouse vocalizations were recorded with a Dodotronic UltraMic 250K 32bits USB 2.0 microphone, with a maximum sampling rate of 250 kHz. This USB microphone is equipped with an on board DAQ and pre-amplifier, and is connected with the acquisition system via USB 2.0. The acquisition of the data and offline processing and analysis was done using custom written MatLab scripts.

## 2e. Pupil size recording

Pupillometry, which is the measurement of pupil size (Nowak et al., 2014), is commonly used for fear recognition in mice, as well as in other animals and humans (Lu et al., 2008). The pupil is driven by the ANS, allowing for evaluation of the visual function with respect to the central and peripheral autonomic systems (Canver et al., 2014; Kandel, 2013). We use pupillometry as a non-invasive technique to record changes in brain state of the animal caused by innate defensive behavior. Our goal was to record real-time ( $\geq 20\text{Hz}$ ) the constriction and dilation of the pupil, i.e. the total area of the pupil, using a custom written algorithm implemented in a C++ script.

For the acquisition of the video frames, a Basler acA640-90um USB 3.0 CCD camera was mounted on a fitting camera holding system by Fisso (type: S-20.00), and pointed on the right eye of the mouse. A commercial bright infrared light (48 LED Light CCTV IR by xx) was mounted on the camera setup to enhance contrast of the mouse pupil. Like most mammals, mice are unable to see infrared light (Cunea et al., 2014), and are therefore not distracted by nor physically responsive to the infrared light. The CCD camera in the setup deliberately lacks an infrared filter, which makes it sensitive to the infrared reflections outside of the pupil, while the pupil itself absorbs the infrared light. The infrared LED does not interfere with the optical imaging equipment either, as the wavelength of the LED (which spectrum lies around 800-900nm), is filtered out by the absorption filter in the optical imaging setup. The CCD camera was equipped with a complementary lens from Basler (type: C125-2522-5M), which has a F-stop setting from F-2.2 to 22 and an initial fixed focus length of 25 mm. The latter was boosted by adding an extension tube to enhance lateral (or transversal) magnification (Fig. 10).



The video acquisition system handles the pupil size measurements, which includes real-time image processing and storage of both numeric, as well as processed video output. Custom written MatLab scripts were used for communication and an external DAQ (by National Instruments, type USB 6008) was used for TTL-synchronization. This process is similar to previously described acquisition systems: information on experiment trial duration and trial data location is parsed into the video acquisition system, when this information is retrieved the acquisition is initiated. The actual acquisition and processing was done by custom build C++ software (using available Basler Pylon C++ Developer API). Both Matlab and C++ source codes can be found in the supplementary.

The algorithm which we used to obtain the pupil area, as well as the x and y coordinates of the center of the pupil, can be decomposed into several steps (Fig. 11). Additionally, a pre-processing step prior to the algorithm and post-processing step at the end were necessary to ensure the correct input and output from and to the algorithm. In the pre-processing step all relevant parameters for the acquisition and image processing are loaded into the program. Followed by a conversion of the original input stream from the USB 3.0 CCD camera

to a gray-scaled image array, enabling the use of the openCV 3.1 C++ libraries for the algorithm. Finally, a region of interest (ROI) was taken from the converted image array and fed into the algorithm.

The pupil size measurements were done with a frame rate of 20 Hz and a ROI, which could be changed during acquisition, for the stream into the algorithm. This stream was processed real-time and could be assed visually by switching on and off streams of different stages of the algorithm. Parameters used in the different stages could be changed during acquisition. This made it also possible to real-time fine-tune algorithm parameters within measurements sessions.

In the first step of the algorithm a Gaussian blur was applied to the image, which has grey-scale values between 0 and 255. This first filtering step is a popular operation in image processing and is essentially used to even small irregularities in the image. Such irregularities could become dominant objects that are tough to eliminate afterwards. The Gaussian filter is low-pass filter based on the Gaussian probability distribution function (McAndrew, 2004) and can be mathematically expressed as

$$f(x, y) = \frac{1}{2\pi\sigma^2} e^{-\frac{x^2+y^2}{2\sigma^2}} \quad (1)$$

Where  $f(x,y)$  contains all data points of the image, and  $\sigma$  is the standard deviation of the Gaussian distribution.

Due to the inevitable reflection caused by the aforementioned infrared illumination, a bright spot is formed on the pupil of the mouse. This light reflex phenomena is also found in humans and is referred to as the Purkinje phenomenal (Lin et al., 2003). In figure 12 four different stages of the algorithm are presented, although the light reflex is not very clear on the Gaussian blur stage, it is very clear on the thresholding stages (Fig. 12B and 12C). To overcome this nuisance, the Gaussian filtering operation was followed by two thresholding operations. The second step in the algorithm. The first thresholding operation is characterized by the following rule

$$f(x, y) = \begin{cases} 0, & \text{if } f(x, y) > \text{threshold} \\ f(x, y), & \text{otherwise} \end{cases} \quad (2)$$

The light inlet of the camera lens (aperture size) is set to slightly saturate the pixels that define the light reflex by the infrared light. The remaining pixels that don't reach the saturation threshold (e.g. 254) remain unchanged. An example of this first thresholding step is shown in figure 12A, the threshold parameter could be changed real-time. This was important, since there were some small changes between measurement session (e.g. exact luminance of infrared light with respect to the eye of the mouse), which have effect on the precise threshold. After the initial thresholding operation the image undergoes a second thresholding operation

$$f(x, y) = \begin{cases} 0, & \text{if } f(x, y) > \text{threshold} \\ 255, & \text{otherwise} \end{cases} \quad (3)$$

The second thresholding operation converted the image stream to a binary form. Which, seriously decreased the size of the image and making it much faster to process. Enabling real-time processing, while maintaining a conveniently large ROI (figure 12B).

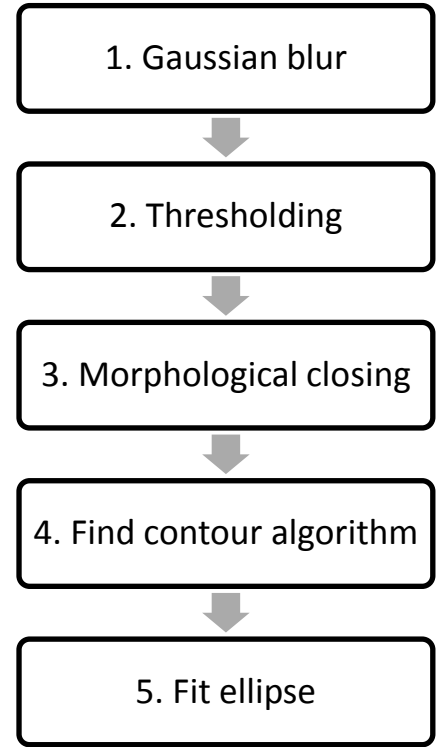


Figure 11 – Pupil size analysis algorithm, in order of task performed. First a Gaussian blur (1) is applied to the image, which is already pre-processed to be parsed into the algorithm. Next, a double thresholding operation is performed (2), whereby the image is converted into a binary type. Morphological closing (3) is added to further deal with a reflection, caused by the infrared illumination. With the find contour algorithm (4), the pupil is detected. This information is passed to ellipse fitting procedure (5). Finally the end result is post-processed and area and x and y coordinates are saved.



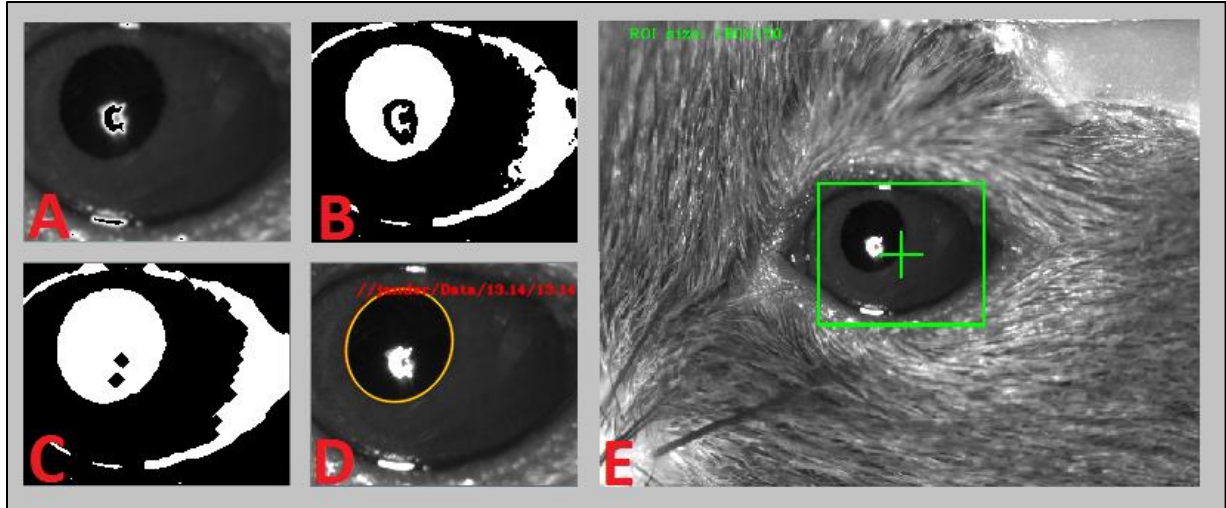


Figure 12 – (A) First thresholding operation, this operation converts the saturated pixels inside the pupil of the mouse to zeros. (B) The second thresholding operating sets a threshold to convert the image stream to a binary form, while preserving the shape of the pupil. (C) Morphological closing deals with the gaps in the pupil, due to the light reflex and whisker movement. It fills up the pupil, which makes it an even elliptical/circular shape. This image stream is finally fed into the last step of the algorithm. (D) An ellipse is fitted to the results from the find contour algorithm and drawn back on the original image stream for visual inspection during acquisition. All relevant parameters concerning these steps could be changed real-time during acquisition.

In the following step a closing operation was introduced to the algorithm, (partially) filling the spot caused by the light reflex (Fig. 12C). Morphological closing, the third step in the algorithm, is a compound morphological operation which first applies a dilation operation, followed by an erosion operation (McAndrew, 2004). Dilation is the union between two matrices, one containing the image data  $A$ , and a matrix called the structuring element  $B$ . The latter is usually a  $n$ -by- $n$  square matrix in the shape of a disc or a square.

$$A \oplus B = \bigcup_{x \in B} A_x \quad (4)$$

The opposite of dilation is erosion, which is the intersect of a matrix containing the image data  $A$ , and a structuring element  $B$ , similar to that described for dilation.

$$A \ominus B = \bigcap_{b \in B} A_{-b} \quad (5)$$

The morphological closing operation can be constructed, by first applying dilation and then erosion to the image data.

$$A \bullet B = (A \oplus B) \ominus B \quad (6)$$

Morphological closing is usually an operation that is performed several times to a binary image, to maximize the closing operation. Although, there is a limit to the maximum amount of iterations, as each iteration adds to the total processing time. For our algorithm we have chosen an elliptic structuring element, inscribed into a symmetrical matrix ranging from 3-by-3 to 9-by-9 (which produces a full circle instead of an ellipse). The maximum number of iterations could be set real-time, although the optimal maximum strongly depends on other parameters such as frame rate and size of ROI. Therefore, a maximum of 10 iterations was set to be the upper limit.

The binary image stream containing the pupil shape, which remained after closing, is then passed onto the find contour algorithm, the fourth step in the main algorithm. The function of the find contour algorithm is to extract the topological structure of a given binary image (Suzuki and Abe, 1983). The find contour algorithm is a method which consists of many operations, which we will not explain in full detail. For a more detailed explanation of this method we refer to the work by Suzuki and Abe (1983). In short, the find contour algorithm



finds the border of an object in the binary image and addresses a label to that border, different objects are labelled and stored accordingly as a vector of points. The last step in our algorithm uses these labelled contours to fit an ellipse. After trying some alternatives, the find contour algorithm turned out to be the most robust method for finding clear edges with the binary image as input. Besides, other edge detectors were found incompatible with the fifth and last step in the algorithm (ellipse fitting). Input to the ellipse fit operation was characterized by three criteria: 1. maximum size of the major and minor axes of the ellipse to be fitted (pixels), 2. minimum size of the major and minor axes of the ellipse to be fitted (pixels), 3. the ratio of the ellipse (size major axes divided by size minor axes). This is a mandatory procedure to discriminate for the pupil contour that shows the most resemblance with the eye of the mouse. The maximum and minimum size of the major and minor axes could be changed real-time during acquisition, remaining parameters could be changed before the experiment if needed.

Finally a circle was drawn on the image stream (Fig. 12D) and saved as visual proof of the pupil size found by the algorithm, which is part of the post-processing step. Before saving the end result video output, this step also adds trial location to the end result. Numerical output: pupil area (pixels), and x and y coordinates of the pupil center; were saved to the location provided by video acquisition system. Additionally, video output could be switched on and off for data reduction. When acquisition is done, the program automatically closes the connection with the USB 3.0 camera and closes all other resources. From that point the video acquisition initiation script in Matlab awaits new trial information. Our proposed algorithm is intended to be a fine balance between speed and accuracy, both needed for a correct pupil size measurement. Relevant parameters used in the algorithm can be found in the appendix.

## 2f. Optical Imaging: wide-field calcium imaging

Wide-field calcium imaging (WFCI) is used as an imaging tool to visualize the areas of the visual cortex of mice, with each area having its own retinotopic map. When neurons are activated, either by chemical (neurotransmitter) or electrical means (depolarization). Electrical activation of a neuron results in opening of the voltage-dependent calcium channels in the plasma membrane. A transient influx of free  $\text{Ca}^{2+}$  in the intracellular space can be regarded as a “Calcium Signal” (Kandell, 2013; Simons, 1988). Intracellular  $\text{Ca}^{2+}$  as a signal regulates cell function in neurons, and is a driving force behind neural communication. The Influx Free  $\text{Ca}^{2+}$ , the *Calcium Signal* is directly related to the spiking (or spike train) of neurons. For this reason it is of interest to study the influx of free  $\text{Ca}^{2+}$  into the intracellular space as a measure of inter-neural communication (Kandell, 2013).

For optical imaging we use a transgenic mice strain with the GCaMP6 indicator present in the visual cortices and the superior colliculus (SC). The GCaMP6 indicator is a recently introduced genetically encoded calcium indicator (GECI) from the GCaMP-family, (Chen et al., 2013; Dana et al., 2014). When excited with light, these indicators absorb and emit light of different wavelengths (Lanni & Keller, 2005; Lichtman & Conchello, 2005; Reichman, 1998). The GCaMP6 indicator increases its fluorescence ( $\Delta F$ ) in response to increases in calcium concentration. The change in fluorescence is usually normalized to background fluorescence ( $\Delta F/F_0$ ) (Chen et al., 2013; Ebner & Chen, 1995; Hillman, 2007; Paredes et al., 2008). When depolarization of a neuron occurs, an influx of  $\text{Ca}^{2+}$  occurs and therefore a larger concentration of free  $\text{Ca}^{2+}$  will inhabit the neuron. This increase in concentrations is the driving force behind the increase in *Calcium signal*, visualized by optical (calcium) imaging.

The active fluorophore in the GCaMP6 indicator is (emerald) GFP, which excitation wavelength is at 489 nm and its emission wavelength at 509 nm (Chen et al., 2013). Fluorescence indicators, such as the GCaMP6 indicator, absorb and emit light, the basic mechanism involves: absorbing a photon of a particular wavelength (light or other electromagnetic radiation) by the fluorescent substance and emitting a photon within the visible spectrum (about 390nm – 700nm), whose wavelength is typically longer (less energy) than that of the absorbed photon (Lanni & Keller, 2005; Lichtman & Conchello, 2005; Reichman, 1998). So when calcium signal increases, due to brain activity in the visual cortices or the SC, this is being observed as a change in concentration ( $\Delta F$ ) with respect to background fluorescence ( $F_0$ ).

An afocal lens configuration of commercially available photographic lenses (Nikon AF-50) was used in a marcoscope setup (Ratzlaff & Grinvald 1991). Such a lens configuration maximizes (Fig. 13), the angle of incidence from the objective and the eyepiece to their corresponding focal points, resulting in the highest possible numerical aperture (NA). When squared, NA becomes a measure of the light gathering capacity of a lens-system, thus a high NA is most advantageous. Beside a high NA, another interesting feature of an afocal lens configuration is constant lateral and longitudinal magnification. The fact that the total magnification of an afocal lens configuration is determined by the fraction of the focal lengths of the lenses, adds to the overall flexibility of the configuration.

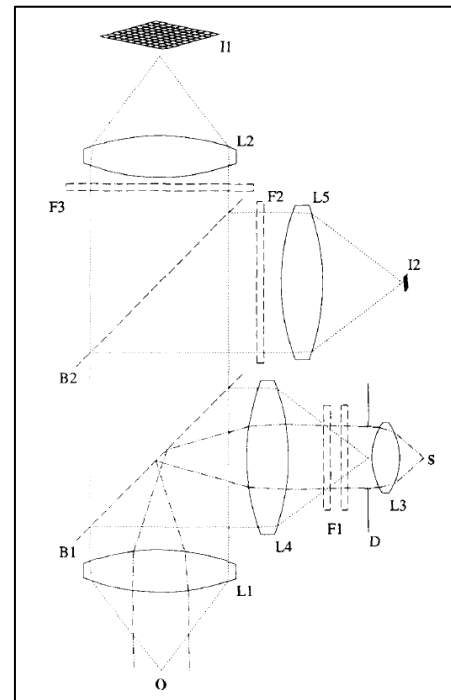


Figure 13 – An afocal lens configuration according to Ratzlaff & Grinvald (1991). The objective L1 and ocular L2 form the afocal combination. In this setup two dichroic mirrors are installed, the first B1 is used for the light source. The second mirror B2 is used to output the signal to a secondary path. The ocular L5 is different from L2 and placed at a different position with respect to L1.

In our macro-scope setup we used a LED light source, which is capable of powerful illumination (Direnberger et al., 2015). The optical band-pass filter has a wavelength of 470 nm and a bandwidth of 40 nm for the excitation of the GCaMP6 indicator. The high-pass optical filter of the dichroic mirror used in the setup, has a 50% cut-off point at a wavelength of 495 nm. An additional optical emission filter was used to block unwanted backscatter. A shutter was used to minimize total light exposure to the brain, which can damage the cell containing the GCaMP6 indicator. The optical image acquisition system waits for a TTL-pulse to be detected and recording starts immediately. This acquisition system was already present at the Heimel lab. No changes were made to either the optical image acquisition hardware or software, besides settings in the software.

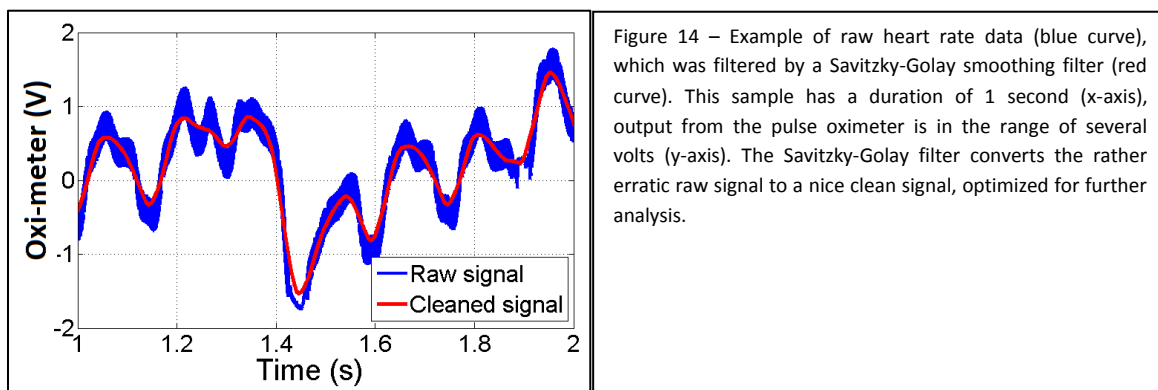
### 3. Data analyses

#### 3a. Heart and Breath rate

Breath rate data was derived from raw heart rate recording data, which was directly recorded from the pulse oximeter. Processing of the raw pulse oximeter signal was done using advanced analyzing functions in Matlab, as well as custom written functions. Deriving breath rate and processing both signals involves several steps, we start by decomposing the processing operations involved in analyzing heart rate:

1. Cleaning the data with a Savitzky-Golay filter.
2. Get trend by convolving cleaned data with a Gaussian function.
3. De-trend raw signal.
4. Apply Hilbert transform on de-trended signal.
5. Find peaks in Hilbert transform.
6. Calculate interval differences (instant heart rate) from found peaks.
7. Calculate average HR (over number of beats).
8. Calculate base, stimulus and post stimulus heart rate averages.

The Savitzky-Golay smoothing filter is a digital filter which is often used on noisy signals whose frequency span (without noise) is large, i.e. a high sampling rate. It outperforms standard averaging finite impulse response (FIR) filters, which tends to also filter out a significant part of high frequency information. Figure 14, shows an example of raw data and filtered data, the filtered signal clearly follows the original, raw signal. Matlab's signal processing toolbox comes with a function called `sgolayfilt()`, which was used for cleaning the signal, additional filter settings of this step and successive steps can be found in the scripts provided in the appendix.



After this procedure, breath rate information could be retrieved by smoothing of the signal, this was done by convolution of the cleaned signal with a Gaussian kernel (similar to the one used in the pupil measurement algorithm). By setting the width of the Gaussian kernel to 750 standard deviation, only low frequency components of the raw signal remained. This signal was used for both analysis of breath rate, as well as for de-trending the cleaned heart rate signal (Fig 15-16).

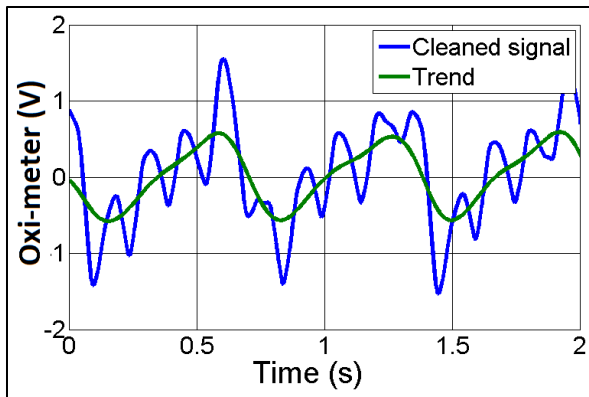


Figure 15 – Example of cleaned heart rate data (blue curve) and trend information (green curve), obtained by convolving the cleaned data with a Gaussian function. This sample has a duration of 2 seconds (x-axis), output from the pulse oximeter is in the range of several volts (y-axis). The trend information is also used for breath rate analysis. In fact the retrieved trend is proportional to the actual breath rate.

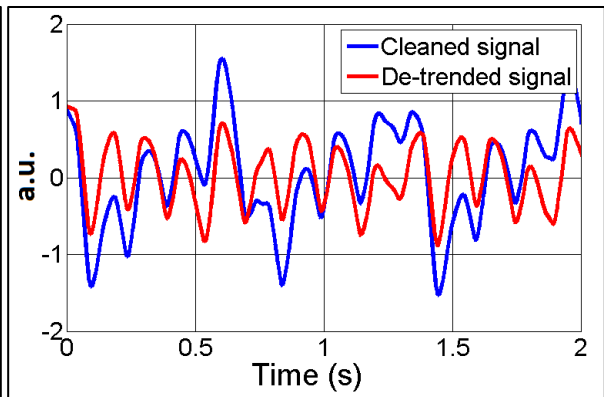


Figure 16 – Example of de-trended heart rate data (red curve) versus cleaned heart rate data (blue curve). This sample has a duration of 2 seconds (x-axis), due to the de-trending procedure the original volt units were lost (y-axis) and are from now on referred to as arbitrary units. The lost units have no effect on the next step in the analysis sequence.

Before the peak finding algorithm could be applied to the data the signal had to be optimized for the `findpeaks()` function from Matlab's signal processing toolbox. Therefore, we used a discrete Hilbert transform on the de-trended signal, and computed the corresponding phase angles. Such an operation is recommended for analysis of spatial information in periodic signals, but beyond the scope of this thesis to explain in full detail. A valuable condition of this procedure is that phase-information of the input signal remains unaltered. Figure 17, shows an example of the output from the fourth step, the discrete Hilbert transforms. The transformed signal is now ready to serve as input to the peak finding algorithm.

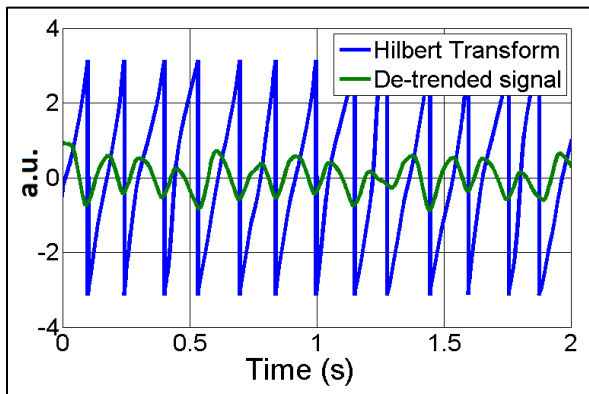


Figure 17 – Example the phase angles of the discrete Hilbert transform (blue curve). The de-trended signal (green curve) served as input to the Hilbert transform. Spatial information is preserved as the negative peaks in the Hilbert transform are fixed to the negative peaks in the de-trended signal. On the x-axis is time in seconds and on the y-axis are arbitrary units.

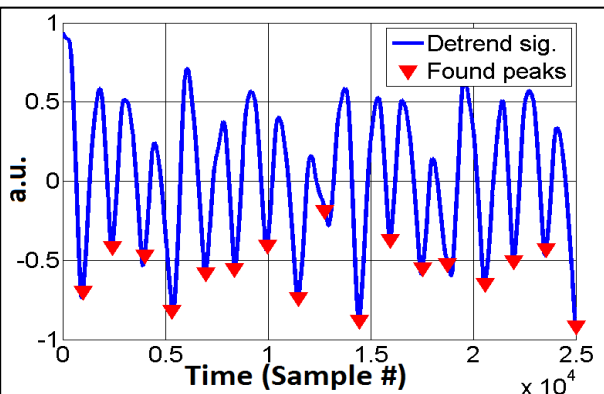


Figure 18 – Examples of peaks found by the peak finding algorithm. In this graph the found peaks (red triangle) are plotted on top of the de-trended signal (blue curve), that served as input to the discrete Hilbert transform. The latter was used to localize peak information. Due to the peak finder algorithm, time couldn't be plot in seconds and is expressed in sample number (x-axis), as well as arbitrary units on the y-axis.

The fifth step in the heart rate analysis sequence, the peak finding algorithm is again a function from Matlab's signal processing toolbox. It returns a vector with the local maxima (peaks) of the input signal vector. A local peak is specified as a data sample that is either larger than its two neighboring samples. The algorithm can be set to find either negative or positive peaks, additionally a minimal or maximal peak distance can be set. We applied a minimum peak height and distance setting to improve robustness of the peak finding step. In figure 18, an example is given of de-trended heart rate data with the results from the peak finding algorithm plotted on the same graph.

Now the exact position is known, an instant heart rate can be retrieved by counting the differences between following peaks, which is done in step six of the analysis sequence. In other words, the instant heart rate is equal to the peak-to-peak interval. From the instant heart rate, an average heart beat was calculated. This average heart beat could be set in a range from an average of 2 beat up to an average of 8 beats, for a more smooth result. Figure 19, shows an example of the intermediate result of step six and seven, these results will serve as the basis for further (statistical) analysis of the experiment data. In the final step (eight) of the heart rate analysis sequence, average heart rates were computed for pre-time (time prior stimulus) recordings, stimulus-time recordings and post-time (time after stimulus) recordings. These averages are used to determine the effect of the threatening visual stimulus on heart rate.

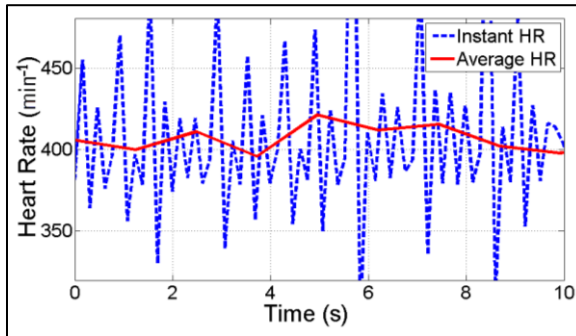


Figure 19 – Example of instant heart rate (blue dotted curve) and average heart rate (red curve). First the instant heart rate is obtained by computing the peak-to-peak interval from the peaks found by the peak finder algorithm. From the instant heart rate, an average heart rate (8 beats in this example) is computed. Both instant and average heart are shown per minute (y-axis), although the scale of the example is 10 seconds (x-axis). Note: the low heart rate was caused by anesthesia, as this example was obtained in an anesthetized mouse.

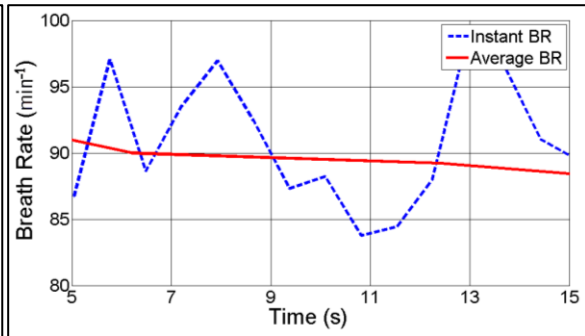


Figure 20 – Example of instant breath rate (blue dotted curve) and average breath rate (red curve). Identical to the heart rate analysis, instant breath rate is obtained by computing the peak-to-peak interval from the peaks found by the peak finder algorithm. From the instant rate, an average breath rate is computed. Both instant and average heart are shown per minute (y-axis), although the scale of the example is 10 seconds (x-axis).

Breath rate was retrieved by step two of the heart rate analysis sequence, convolving the cleaned heart rate signal with a Gaussian function to extract low frequency information. Breath rate was analyzed identical to heart rate from the heart rate analysis sequence step four and onwards. Figure 20, shows an example of an intermediate result of breath rate at step seven of the sequence.

### 3b. EMG

When digitized the EMG signal was already filtered by a band-pass filter (low cut-off: 100Hz, high cut-off: 1000Hz), built into the amplifier. The analysis of EMG data (Fig. 21) was done by first rectifying the raw signal and secondly by smoothening of the signal. Rectification is a common processing step in the analysis of EMG data (Neto and Christou, 2010), we implemented this by taking absolute value of each data point ( $x$  represent the raw EMG signal):

$$y(x) = |x| \quad (7)$$

Subsequently, a smoothing operation with a time-frame set at 25 milliseconds was applied to the rectified signal. We used the `smooth()` function from Matlab's curve fitting toolbox. This operation smooths the data using a moving average filter.

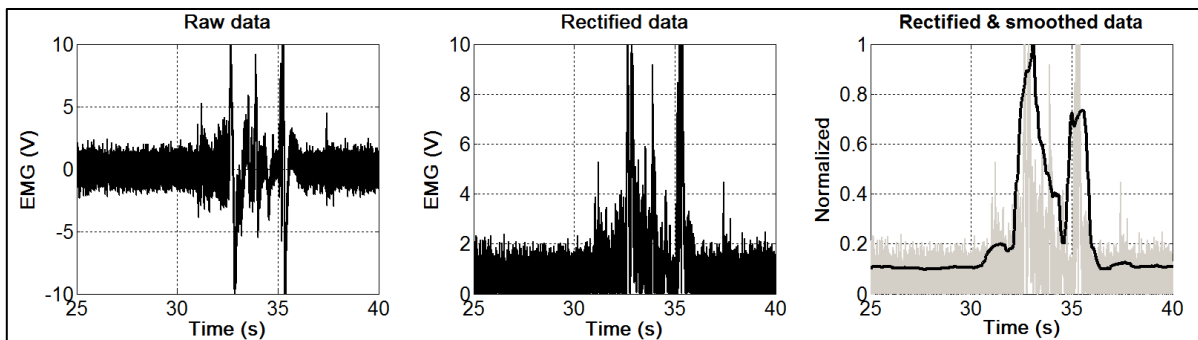


Figure 21 – On the left, Raw EMG data was recorded in volts (y-axis) and is plotted against time in seconds (x-axis). The raw EMG data was rectified (middle graph), so that no negative data remained, the units on the y-axis are in volts and on the x-axis time in seconds. On the right, an example of smoothed (25 ms time-frame) rectified EMG data (right graph). The smoothed signal (black curve) represents tightly the envelope of the rectified data (gray curve). Both the rectified as well as the rectified and smoothed signal were normalized for the example.

To compare the EMG data with the results of the video recordings, which had a sample rate of 20 Hz, the signal had to be resampled (by taking every  $n^{\text{th}}$  sample of the original signal). Next, mean values for the duration of the stimulus and duration of pre and post stimulus time were calculated.

### 3c. Ultrasound

While ultrasound was recorded during acquisition, no consistent analyzing was done due to ambient noise constraints. Although, some data was looked into briefly to explore the possibilities of further analysis of this data. In this preliminary analysis we took the spectrogram (Fig. 22) of the (ultra)sound, revealing the vocalization by the mouse, shortly after its head was fixed.

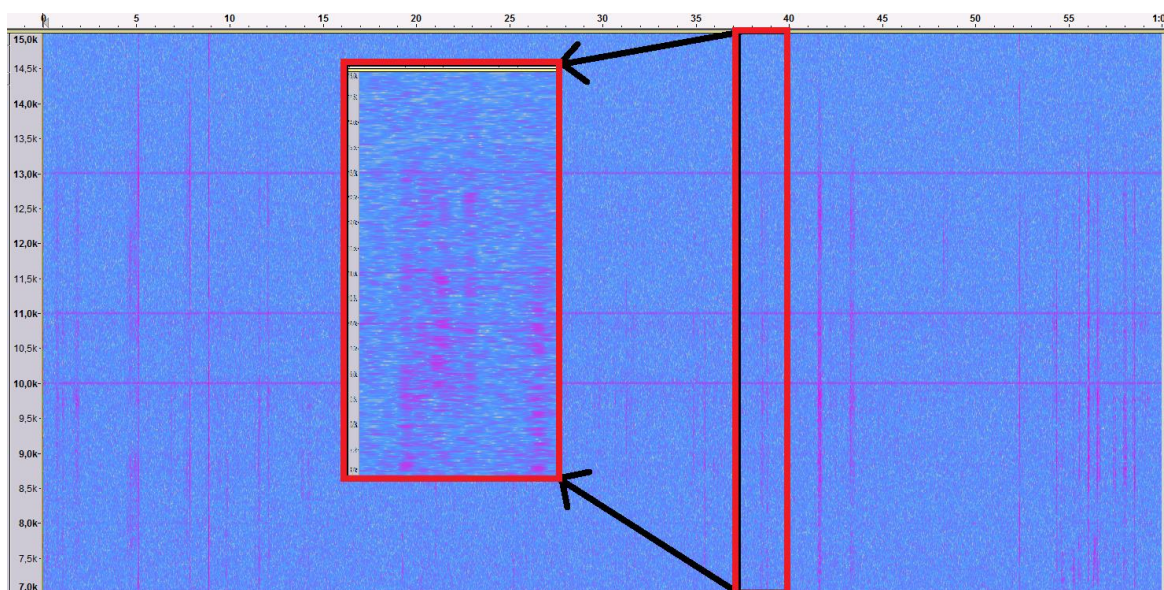


Figure 22 – spectrogram example of (ultra)sound recording. On the y-axis the frequency range (from 7kHz to 15 kHz), and on the x-axis time in seconds (from 0 to 60 seconds). Inside the red box the recorded vocalization from the mouse. The purple areas indicate an increase in the power spectrum at that give frequency and time. Both boxes share the same span of x-axis (although they are scaled differently).

The spectrogram shows changes in the power spectrum of sampled (ultrasound) data at a given frequency (Hz) and time (s), by gradually changing color as more activity occurs. In this example the color turns to purple as more activity is detected in the (ultra)sound data.



### 3d. Pupil recording analysis

Numerical output of the algorithm, used in the assessment of the area and x and y coordinates of the pupil, were stored and smoothen in Matlab. This was a necessary step, since the algorithm could provide a zero output when no ellipse (5<sup>th</sup> step of the algorithm) could be fitted. These zeros in the output are thus added artificially and do not reflect the actual size or change of position of the pupil. In most cases the zeros are added because the mouse blinks or the pupil is in the far corner of the eye. The latter causes the pupil to form a shape that exceeds the maximum preset elliptical ratio. This artificial contribution of zeros is an unwanted byproduct of the algorithm and was dealt with by interpolating the missing number and using Matlab's smooth() function, which is part of Matlab's curve fitting toolbox. This function filters data using a moving average filter, set between 750 milliseconds and 1.25 seconds (e.g. 15 to 25 frames, at a frame rate of 20 Hz). The result of this operation is a continuous curve that accurately follows the original pupil size trace. Figure 23 shows an example of the operations performed on the pupil area signal. Eventually the signal was normalized for further analysis.

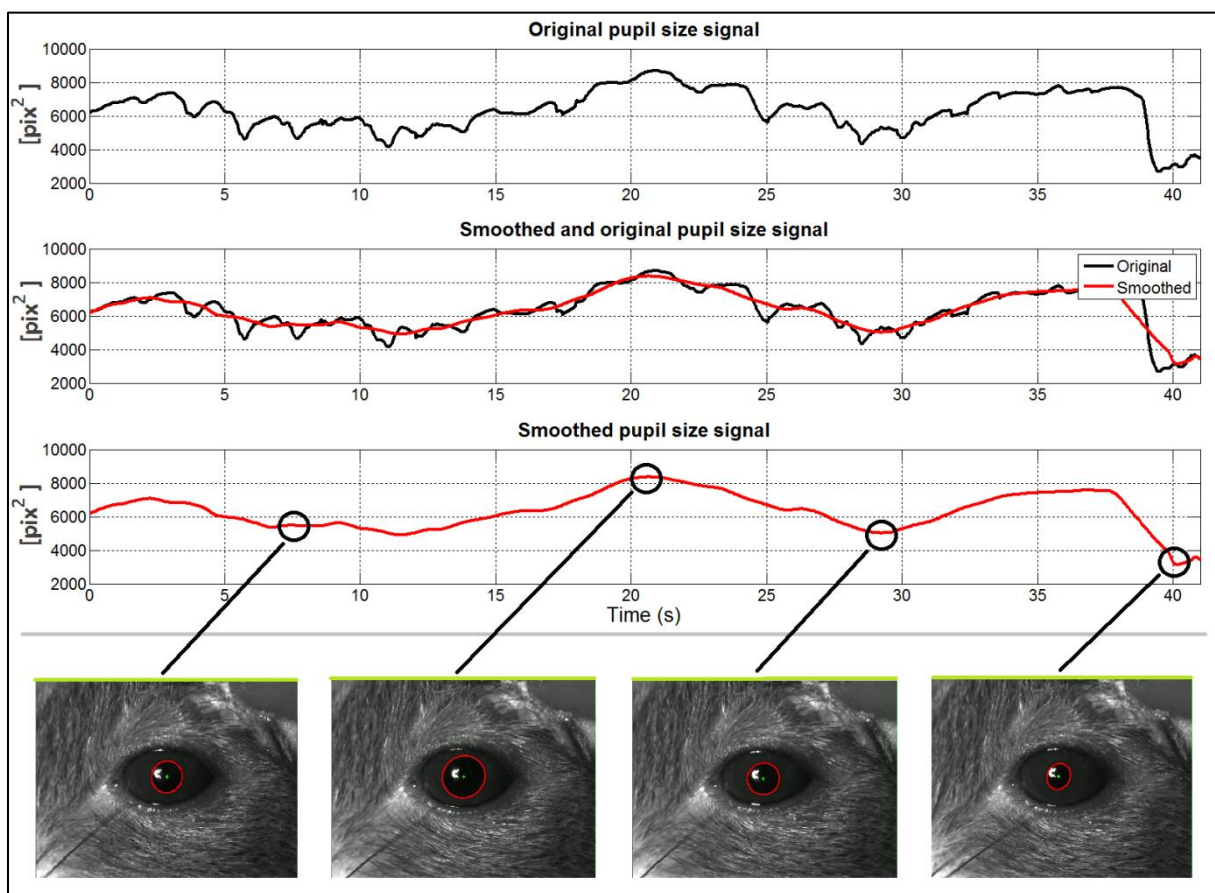


Figure 23 – on the y-axis the area size in pixels, which is plotted against time (s) (x-axis). The first graph on the top is the original signal, the zero results were replaced by NaN values (instead of a continuous curve, there are little gaps in the curve due to the NaN values). The middle graph shows the original signal (black) and the smoothed result (red). In this smoothing operation a moving averaging filter was used, averaging the original signal over 2.5 seconds (50 frames). The timeframe used for these examples was higher (for illustrative intentions), than used for the experiments. By smoothing the signal (with the NaN replaced values), the signal became continuous again, and therefore more robust for analyzing time averages. The last graph shows only the smoothed signal, below it on the x-axis some video snapshots referring to the pupil size signal at various moments. The different snapshots show that the elliptical ratio of the fitted ellipse ranges between 1 and some preset number (ratio  $\leq 1.5$ ). Total pre, post and stimulus time were later used to further analyze the smoothed pupil size signal.

The x and y coordinates of the center of the pupil were analyzed using the same operations as the area of the pupil. In Figure X, the first and second graph are the normalized derivatives of the x and y position recordings (defined as  $f(x)$  and  $f(y)$ ). Interpolation and smoothing were necessary as there could be some 'faulty' detection of the pupil during acquisition. To determine the relative change we used the following method

$$\text{Relative change } (x, y) = \sqrt{(dx)^2 + (dy)^2} \quad (8)$$

This way of analyzing the signal has proven to a robust method as it follows the pupil as can be seen in the videos recordings (Fig. 24).

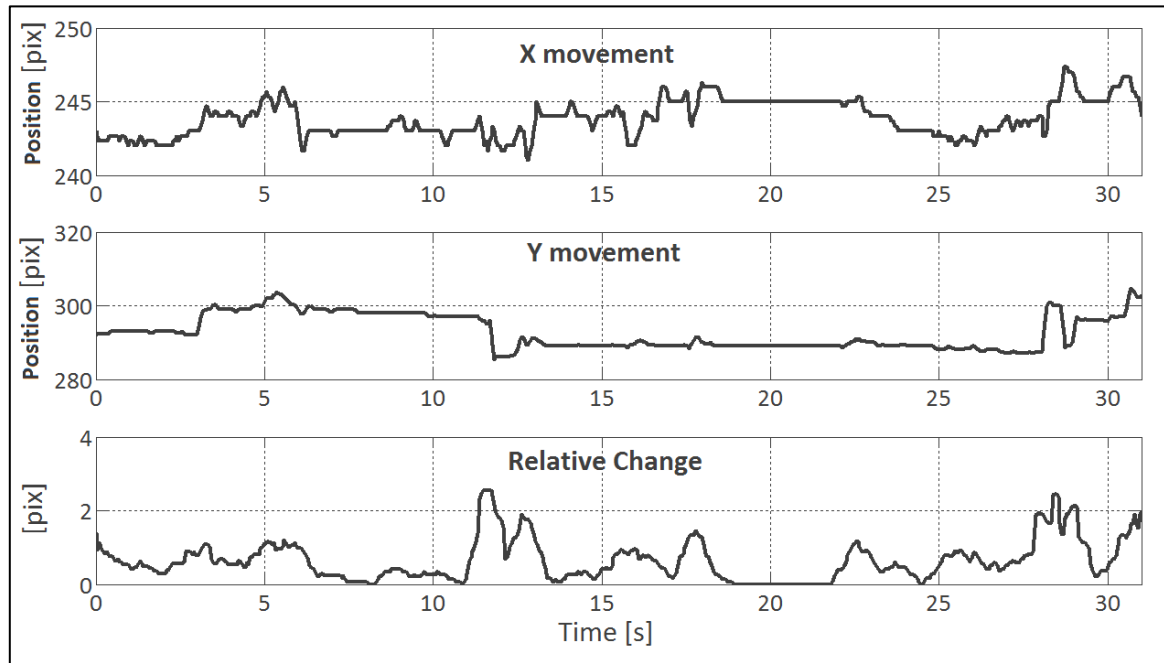


Figure 24 – The first two graphs shows the X and Y position of the pupil. A smoothing operation with a timeframe set at 15 frames was applied to the raw data, afterwards the relative change was calculated, shown in the last graph.



## Results

We obtained data on two sets of stimuli, which results are presented separately. First, we present results in which we validate the implemented acquisition and analyzing method, but also investigate the relations and correlation among several data types. This was done by showing a strong change in luminescence on the stimulus screen (instantly from 0% to 100% and black). The second set of results are of equal importance. These results were acquired with a looming stimulus, and will be used in determining baseline criteria for the extended research goals as described in the introduction. Similarly, the relations and correlation among several data types were explored and identified.

### 1. Validation experiment

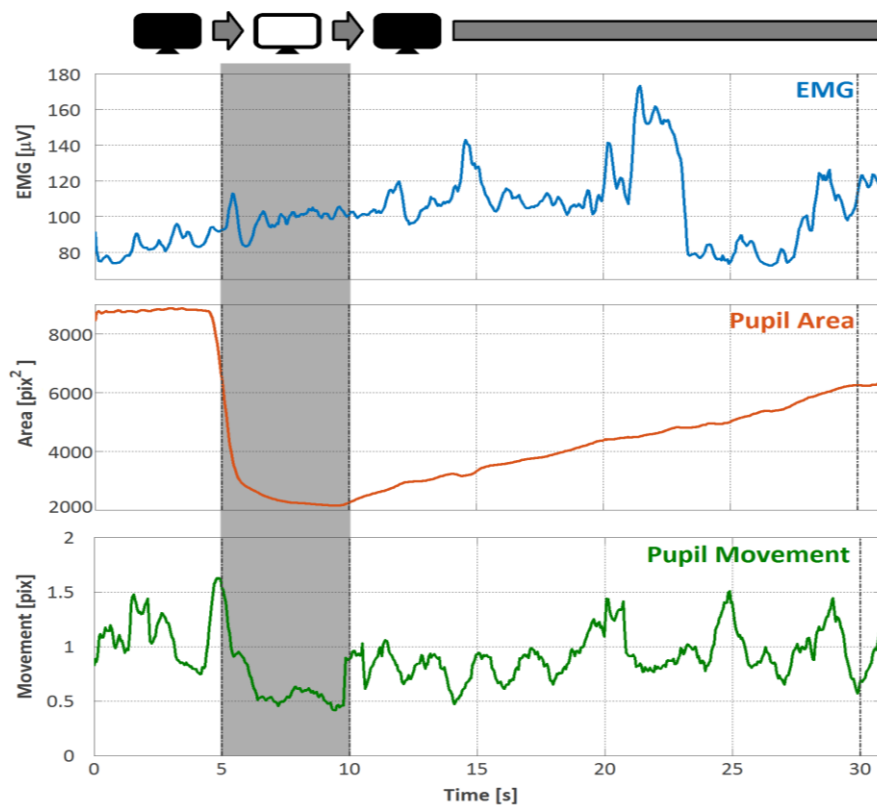


Figure 25 – Overview of different observed overall average activity during validation experiments (n=13). EMG activity (blue), expressed in microvolts ( $\mu\text{V}$ ). Pupil constriction and dilation activity (orange), expressed in  $\text{pixels}^2$ . Relative pupil movement activity (green), expressed in pixels. The first 5 seconds the screen is black, followed by 5 seconds of 100% luminance (gray area). At that point the screen switched back to black for a period (at least) 21 seconds.

To analyze physical responses in an awake animal it is crucial to know the relation and reaction to stimuli among different recorded responses, as well as the reaction of the animal to the experiment in general. We choose to include the validation part in the results section, as analysis of these results function as a measure for interpreting stimuli that evoke innate defensive behavior in the mouse. The type of stimulus used in these validation experiments was designed for recording physical responses of the mouse to a strong change in luminescence coming from the screen above the mouse. Each trial starts with 5 seconds of pre-time, in this interval the whole screen is set at 100% black. After the pre-time, the stimulus starts and the screen jumps to 100% white, introducing a

strong instantaneous change in luminescence. The stimulus is on for 5 seconds and then jumps back to the same state as it was in during pre-time. Additionally a long post-time interval of 20 seconds was added to the recording time of each trial. During these validation experiments the optical imaging (OI) equipment was removed, which provided more room directly above the mouse for the stimulus-screen, and so a sufficient overhead panorama for the mouse to react to.

The result of the different signals after processing and down-sampling are shown in the graphs of figure 25. The gray area through the graphs indicates the start of the stimulus at 5 seconds and the end of the stimulus at 10 seconds. The pupil size clearly reacts strongly to the sudden brightness of the stimulus, by contracting from maximum (8865 pix<sup>2</sup>) to a minimum (2153 pix<sup>2</sup>) position a very short time (due to averaging and smoothing), just before 5 seconds. Raw individual trial data reveals that a 50% drop in total area size can be accomplished within 250 milliseconds. It is evident that such a decrease will not be seen in the cumulative data from the validation experiments as this information was averaged out. After 10 seconds the pupil area size slowly increases, up till the point the recording stopped. Individual trial recordings which had a post-time of 30 seconds show that a 50% recovery of pupil area size took around 25 seconds. The EMG signal increases over the greater part of the time course, while pupil movement clearly was reduced to a minimum throughout the stimulus interval.

For further comparison between the signals, the post-time interval of the average trial data was normalized by a rescaling operation to match the time scale of the pre-time and stimulus on-time. Each graph in figure 26 shows data per signal type, so that differences among the successive interval times can become visible in these close-ups. The EMG interval times graph illustrates the change in mean of post-time EMG activity compared to stimulus time, which is significantly higher. Directly after the stimulus was shown the average pupil movement activity dropped significantly by 41% for the entire stimulus interval. The data was checked for a normal distribution with a KS-test, which gave a positive result. Hence, a non-parametric Wilcoxon signed-rank test was used to test for significant interval differences (see appendix for detailed results).

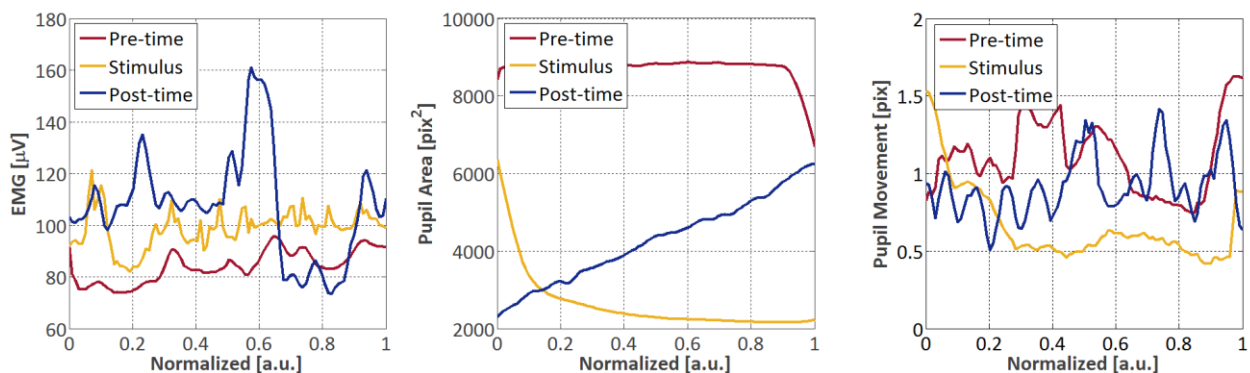


Figure 26 – Overview of different average interval times from the validation experiment (n=13): pre-time (red), stimulus-time (yellow) and post-time (blue). EMG activity is expressed in microvolts (μV), pupil constriction and dilation activity is expressed in pixels<sup>2</sup> and relative pupil movement activity in pixels. Post-time was rescaled to match the time scales of the pre-time and stimulus-time. Consequently time information was lost and normalized between 0 and 1.

The results of the Wilcoxon signed-rank test are shown in the box-plots (Fig. 27) below, the gray bars indicate the mean of the signal per time interval (standard error of the mean (SEM): red lines in graphs). All differences among the pupil size time intervals were considered highly significant

( $p < 0.001$  &  $p < 0.01$ ), see appendix for detailed test results). There is also a significant difference between the mean EMG pre-time and stimulus-time, as well as the EMG pre-time and post-time ( $P < 0.01$ ). The clear drop in the average pupil movement activity at the stimulus onset, lead to a significant difference between the mean pre-time interval and mean stimulus-time ( $P < 0.001$ ). These differences underline what is observed when looking at the graphs of figure 25 and 26, and indicate that the physical state of the animal before the stimulus onset differs from that during stimulus and/or recovery.

We investigated how many additionally trials would be necessary before non-significant differences would become significant. Power analysis estimations (set at an accuracy of 80%) for the EMG and pupil movement activity indicate 20 additional trials would be needed for the mean stimulus-time and post-time to become significantly different ( $P < 0.05$ ). Assuming that the recorded mean interval times were truly a reflection of the real differences. The remaining interval time combinations needed more than 25 additional trials to become significantly different (detailed result can be found in the appendix).

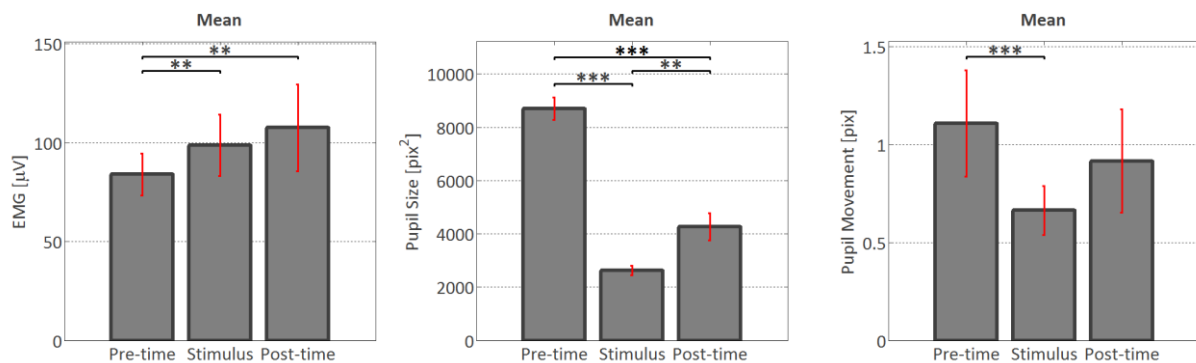


Figure 27 – Results mean interval times validation experiment. Average trial data was subjected to a goodness-of-fit test (Kolmogorov-Smirnov test / KS-test) to check if the data was normally distributed, which gave a positive result. The standard error of the mean (SEM) is expressed by red vertical lines. EMG activity is expressed in microvolts ( $\mu V$ ), pupil constriction and dilation activity is expressed in pixels<sup>2</sup> and relative pupil movement activity in pixels. Significance: \*\*  $p < 0.01$ , \*\*\*  $p < 0.001$ , was tested with a Wilcoxon signed-rank test ( $n=13$ ).

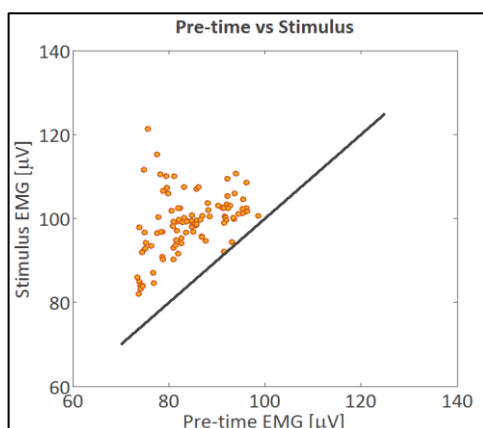


Figure 28 – Scatter-plot of mean EMG pre-time interval plotted against the mean EMG stimulus-time. EMG activity is expressed in microvolts ( $\mu V$ ).

The SEM in the box-plots of the mean EMG signal indicate a possible mistake in the statistical approach of testing for significance. As the data was non-normally distributed the SEM might give an imprecise impression, when interpreting the statistics. Therefore we looked at the relation between the EMG interval times by evaluating their respective scatter-plots. An example of such in figure 28, this is a scatter-plot of the average pre-time EMG activity compared to the average stimulus-time activity. The evaluation of the observed scatter-plots supports the statistical significance found by the Wilcoxon signed-rank test.

Another interesting point that could be made when inspecting the graphs of figure 25, are the visible correlations among the different signals throughout the time course. We looked at the cross-correlations of all trials and calculated the mean cross-

correlation result for each interval time comparison. Although (cross-) correlations between signals were not very strong, there were significant correlations at 2 standard deviation (SD). A significant negative maximum correlation of -0.12 was found at a lag of 150 milliseconds between the EMG signal and pupil size data. The EMG signal has a positive significant correlation of 0.23 at a lag of 500 milliseconds with respect to the pupil movement data. Pupil movement activity compared to pupil size had a maximum correlation of 0.20 and at negative lag of 850 milliseconds. Differences between the different signals and time intervals are evident in these validation experiment results. Normalized pupil area time intervals show significant differences, whereas the overview in figure 25 reveals detailed reaction of EMG, pupil size and pupil movement changes throughout the time course of the average response.

## 2. Looming disc measurement

This second part of the results section is dedicated to results obtained by trials from sessions in which an overhead looming stimulus was presented to the mice. These results will contribute to the baseline criteria of reactions to threatening fear evoking stimuli, like a looming disc. Changes in the physical state of the mouse were captured by means of EMG recordings, pupil area size and movement recordings, ultrasound recordings. In this part the looming disc stimulus used was described in detail in methods section 2a. The pre-time and post-time in these trials was set at 3 seconds, total stimulus-time was set at 7.5 seconds. First we show the response of the mouse to the stimulus in an individual trial example, and we focus on the interaction among signals. Finally we conclude our results by showing our main results, which are the stimulus session cumulative results. These experiments took place over a time span of 4 nonconsecutive session days, with a total of 50 trials of which 45 were included into the analysis prior to these results.

### 2a. Individual trial result

Before we introduce the session results it is meaningful to first look at an individual trial from the looming disc experiment sessions. Individual trial results could reveal information that is lost when looking at an average response over many trials among various sessions. We have selected an example trial to further investigate and which is representable for the majority of the trials used. The aim of showing this individual trial results is to focus on the time course and interaction among EMG activity, pupil size change and pupil movement activity. The data was processed, normalized and down-sampled for visual comparison.

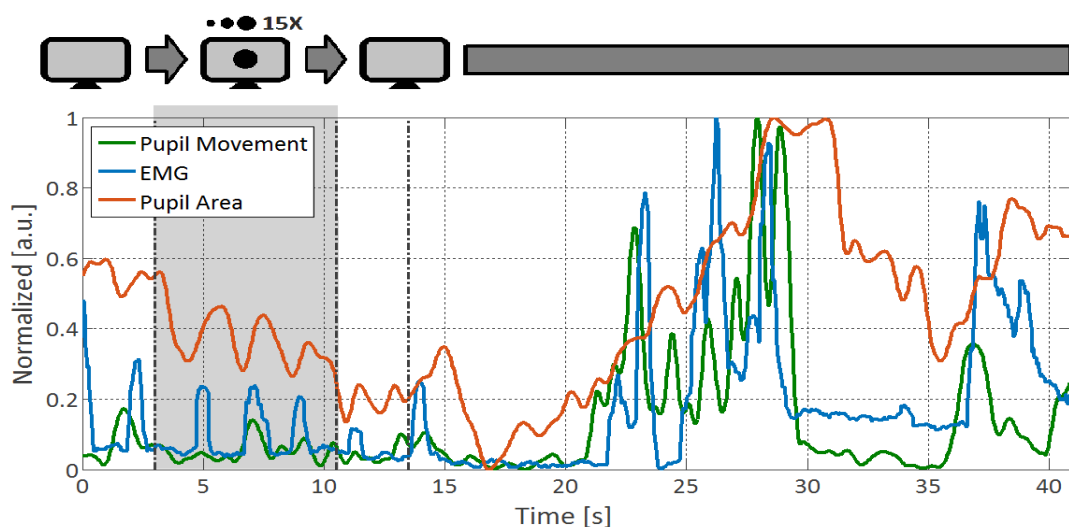


Figure 29 – Overview signals individual trial example stimulus session. EMG activity (blue). Pupil constriction and dilation activity (orange). Relative pupil movement activity (green). The first 3 seconds the screen is 25% gray, followed by 5 seconds stimulus (gray area). At that point the screen switched back to 25% gray for a period (at least) 31 seconds. The post-time had a duration of 3 seconds. The data was normalized (between 0 and 1) for visual inspection of the different signals on a joint y-axis.

The results of this individual trial example are shown in the graph of figure 29, which contains an overview of normalized EMG activity, pupil change and pupil movement activity. The onset and end of the stimulus is indicated by the gray bar in the graph at 3 and 10.5 seconds. The graph contains some interesting information on how different (changes in) signals interact over the course of time. Peaks in the EMG, pupil size or pupil movement signal reflect a direct change in the observed behavior of the mouse, in contrast to cumulative data such as the validation results. In this example

the signals seem to be locked in time, but also in (normalized) size. Pupil movement and EMG signals show a strong visual similarity, however we stress that the signals in graph 29 were normalized between 0 and 1 for illustrative purposes. The degree of constriction and dilation of the pupil shows a much more gradual slope compared to EMG or pupil movement and does not lock to the other signals from 32 till 35 seconds.

Similarity among the signals of the individual trial example was further investigated and cross-correlation results (Fig 30) were examined. All signals show a moderate to high ( $>0.6$ ) positive correlation at a significance of 2 SD (gray dotted horizontal lines). When EMG activity is compared to pupil size change, the signals had a maximum correlation of 0.65 at a positive lag of 1.0 second. EMG activity compared to pupil movement activity had a maximum correlation of 0.62 at a negative lag of -400 milliseconds. Cross-correlation results between pupil movement and size revealed a maximum correlation of 0.66 at a positive lag of 1.65 seconds. Differences between mean cross-correlation results were also considered highly significant ( $P < 0.0001$ ).

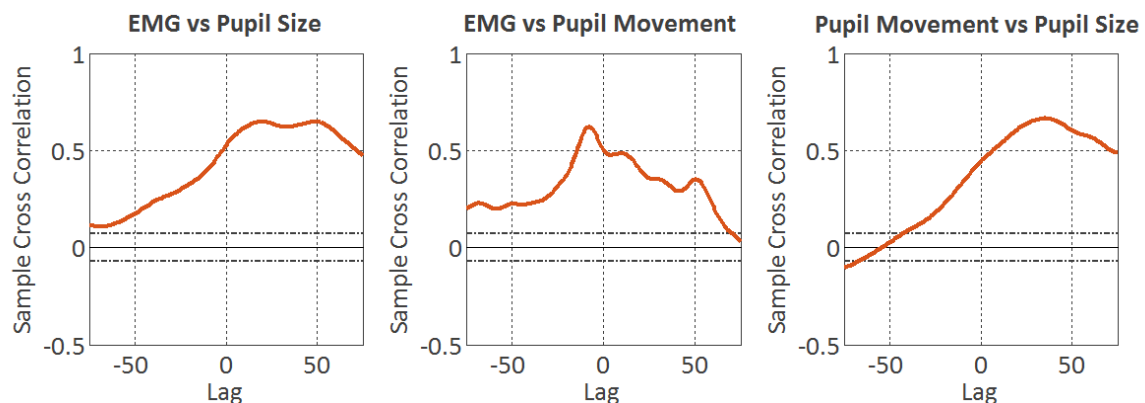


Figure 30 – Cross-correlation results from different signals of the individual trial example. EMG activity, pupil constriction and dilation, as well as pupil movement were examined. Correlation ( $\rho$ , y-axis) between these signals is plotted against the lag of the found correlation (x-axis, lag is equal to the sample rate of the processed signals, 20 Hz). Gray dotted lines indicate significance at 2 standard deviation.

## 2b. Session results

Before the signals could be analyzed for comparison and exploration of the effect of the stimulus on the mouse, the raw data was processed and down-sampled and individual trials were checked to exclude trials which contained corrupt data (e.g. due to hardware failure). Setup parameters did slightly alter between measuring sessions (e.g. distance of the camera to the pupil), which introduced variations in mean signal and possibly the reduction of (some) individual trial responses. Nevertheless, we managed to sum up all 45 preselected trials for analysis of the average signals relating to the repeating looming disc stimulus.

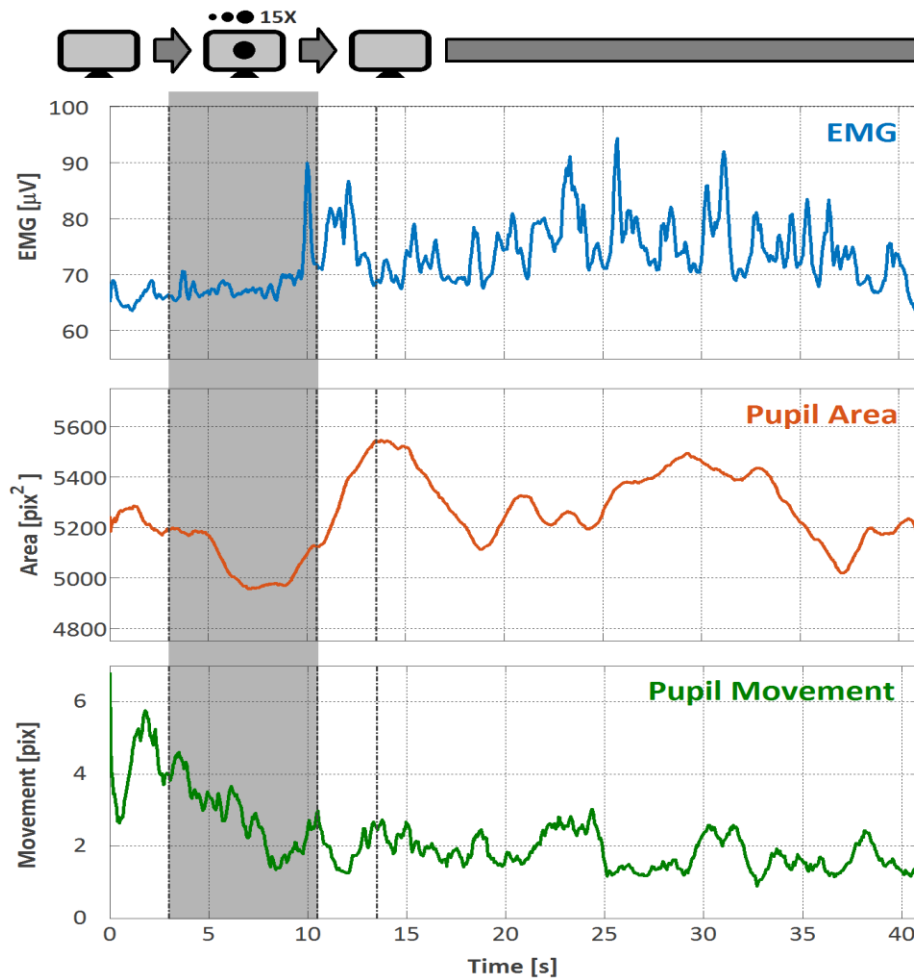


Figure 31 – Overview of different observed average signals in the stimulus sessions (n=45). EMG activity (blue), expressed in microvolts ( $\mu\text{V}$ ). Pupil constriction and dilation activity (orange), expressed in  $\text{pixels}^2$ . Relative pupil movement activity (green), expressed in pixels. The first 3 seconds the screen is 25% gray, followed by 5 seconds stimulus (gray area). The stimulus had 15 repetitions of a looming black disc and at the end of the stimulus the screen switched back to 25% gray for a period (at least) 31 seconds. The post-time had a duration of 3 seconds.

Signal averages of trial results are shown in the graphs of figure 31. The onset of the stimulus is indicated in the graphs by the gray vertical bar at 3 seconds and 10.5 seconds. The most notable effect is caused by the constriction and dilation of the pupil, during and after the stimulus presentation. The peak dilation after the recovery onset lies around 13.5 seconds, but decreases almost as fast afterwards to pre-stimulus values around 19 seconds. Following this first peak in pupil size after the stimulus was shown, the pupil size again increases, but the slopes of both sides of the curve is far less steep and is not considered relevant to the analysis (at this time) as it lies outside the

interval times. Another salient detail is the increase in EMG activity, around the onset of the recovery interval. Not only was there significantly more overall EMG activity during and after the stimulus compared to pre-time interval, the signal becomes also more erratic (less smooth compared to the time before the onset of the post-time). The pupil movement activity decreases rapidly but not significantly at the onset of the stimulus, which matched our visual observations of the mouse during the experiments.

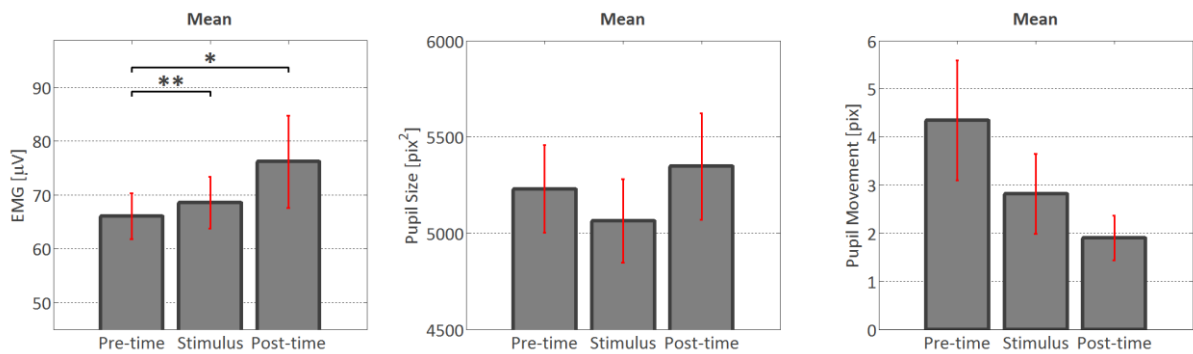


Figure 32 – Results mean interval times stimulus experiment. Cumulative session data was subjected to a goodness-of-fit test (Kolmogorov-Smirnov test / KS-test) to check if the data was normally distributed, which gave a positive result. The data was compared using a Wilcoxon signed-rank test ( $n=45$ ). Significance: \*  $p<0.05$ , \*\*  $p<0.01$ . The SEM is expressed by red vertical lines. EMG activity is expressed in microvolts ( $\mu\text{V}$ ), pupil constriction and dilation activity is expressed in pixels<sup>2</sup> and relative pupil movement activity in pixels.

The mean interval time results of the average signals are presented in the box-plots of figure 32 and support the observed differences before. Overall EMG activity rises with each successive interval, with the largest consecutive increase between the stimulus-time and post-time. Both pre-time and stimulus-time, as well as pre-time and post-time were found to be significantly different ( $p<0.05$  &  $p<0.01$ ). The mean values of the pupil size interval times (middle bar plot) signals an important (non-significant) difference before and after the stimulus is shown. At this interval the mean pupil size shows an evident decrease (constriction). Overall pupil movement decreases clearly from pre-time to post-time.

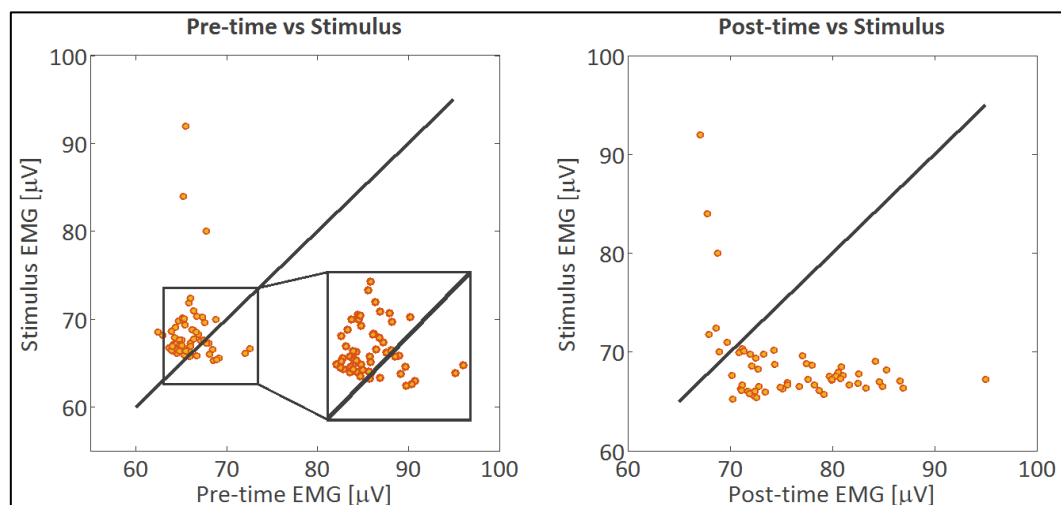


Figure 33 – Scatter-plots average EMG signal: (left) mean pre- and stimulus-time interval; (right) mean post- and stimulus-time interval. EMG activity is expressed in microvolts ( $\mu\text{V}$ ). There are no hidden data points behind the close up in the left graph.



Scatter-plots of the were included to confirm the (mean) interval time results from figure 32. Special attention was given to scatter-plots of the EMG signal. In figure 33 we show both pre-time plotted against stimulus and stimulus plotted against post-time values. The spread of the data points in the post-time vs stimulus scatter-plot exposes the origin of the non-significant difference (as a large variation in data points yields non-significant test outcomes). Additionally we investigated the number of extra trials which would be needed to be included to the existing sample pool (assumed that the recorded mean interval times were truly a reflection of the real differences), to yield a significant ( $p < 0.05$ ) result between the mean signals of the non-significant interval times. Power analysis estimations (80% accuracy) are tabulated in the table below.

	EMG	Pupil Size	Pupil Movement
Pre-time vs. Post-time	0	>50	0
Pre-time vs. Stimulus	0	>50	10
Post-time vs. Stimulus	46	39	12

Table 1 – Power analysis: the number of additional trials needed before a 80% of that number is statistical significant ( $p < 0.05$ ), results >50 were dismissed.

Besides differences between interval times, we also looked at the correlations between the EMG, pupil size and movement to quantify their interaction throughout the time course. Cross-correlation results of all trials were sampled and the mean cross-correlation results are presented in figure 34. The first cross-correlation result (left) exposes a positive correlation of 0.23 between EMG activity and pupil size. The EMG signals seems to lead with respect to the pupil size, by a positive lag of 650 milliseconds. Cross-correlation results from the EMG activity and the pupil movement show that the EMG and pupil movement had a maximum correlation of 0.20 at a negative lag of -550 millisecond, which implies correlated increase in EMG activity when there is a rise in pupil movement activity. Pupil movement compared to pupil size had a maximum correlation of 0.18 at a positive lag of 1.25 seconds. These cross-correlation results are less evident than those found in individual trial examples, which is primarily due to the averaging of the signal over many trials.

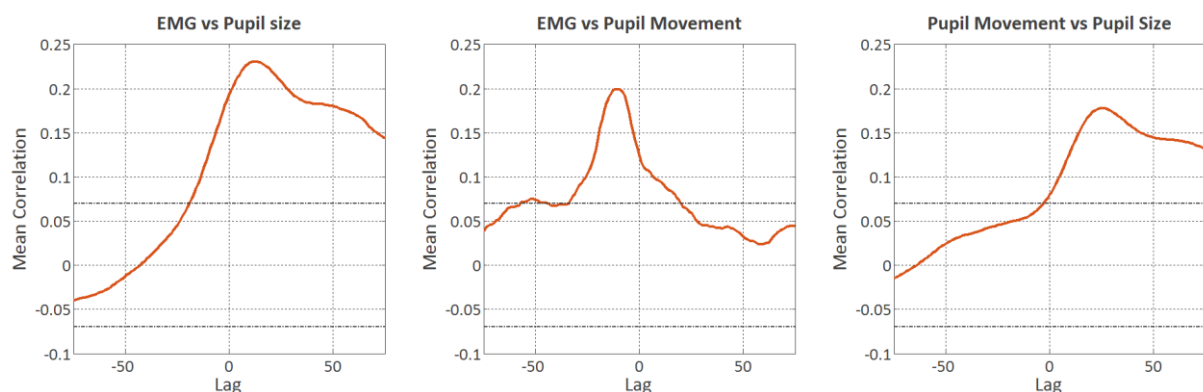


Figure 34 – Cross-correlation results from different signals of the samples average session data. EMG activity, pupil constriction and dilation, as well as pupil movement were examined. Correlation (Rho, y-axis) between these signals is plotted against the lag of the found correlation (x-axis, lag is equal to the sample rate of the processed signals, 20 Hz). Gray dotted lines indicate significance at 2 standard deviation.

Following the cross-correlations results and after observing the signal overviews in figure 30, there seems to be an order of delay between the different signals. Pupil movement seems to lead in terms of the onset to an event, which is followed by the EMG activity. Constriction or dilation of the pupil

can be considered to lag the most with respect to the other signals. However, detailed analysis on time constants (e.g. rise and fall time of the pupil size change, or time constants between cross-correlation results of individual trials) among individual trials or signal averages has not been done (due to time constraints). We observed a difference between the cross-correlation results of the validation and repetitive stimulus experiment. In the latter only positive maximum correlations occurred, while there was a negative maximum correlation in the strong stimulus locked validation experiment. This also had an effect on the order of (time) delay between the maximum cross-correlation results.

Besides recording EMG activity, pupil size and pupil movement activity, an attempt was made to record heart rate fluctuations. This was done in some previous (awake and head-fixed) trials, which were not included in the stimulus experiment analysis discussed in this section. For these recordings we introduced the pulse-oximeter as mentioned, which makes use of a collar-sensor and was positioned around the neck of the mouse. Only for brief moments, mostly less than a second, the pulse-oximeter provided a usable output that could be used in the processing of the signal as described in the methods section. This lack of usable data prohibited the processing steps necessary prior to the analysis of the data. We would also like to mention that ultrasound recordings were recorded among all trials, but couldn't be used for further processing. This was caused by too much ambient noise and various sounds had become indistinguishable when recorded. These poor results from both heart rate and ultrasound recordings were neglected in the analysis of this study, but will be discussed in the next section.

## Discussion

Our study was aimed to design an experiment setup with capabilities to capture brain activity and physiological change, as a function of innate defensive behavior in response to different types of (threatening) looming stimuli. By acquiring preliminary data with this newly built setup, we investigated the reaction of the mouse to the experiment setup, as well as the strength of the employed method for registering changes in physiological change. Furthermore we evaluated the reactions of the mouse to (threatening) stimuli and established probable baseline criteria for further research. Lastly, we reflect on some ambiguities within the present experiment setup and method and administer our thoughts on how to improve functionality.

We designed an experiment setup and method for in vivo recording, including: heart, respiration rate, EMG activity, pupil size, pupil position and alarm calls. The setup included also an optical imaging (OI) device which shall be used for investigating the areas of the visual cortex in experiments to come. Considering the awake state of the mice and the desire to implement OI, the mice needed to be restrained and head fixed (visual and graphical examples of the experiment setup are shown in figures 3 and 4). Results from the validation (mostly) and stimulus experiments increased our expectations of the usability of the applied setup and method. Before any experiment could be conducted, the setup was tested and evaluated extensively throughout the course of this research project. Within the boundaries of this project OI is not thought to be a relevant asset to investigate, as the present OI setup is actively used in similar imaging experiments (head fixed, with a clear imaging skull-window).

With this newly designed experiment setup, two sets of data were acquired: a validation experiment dataset and a stimulus experiment. The validation experiment used a strong light reflex to stimulate reflexes of the autonomic nerve system. Results of these experiments showed, as expected, strong reactions to the sudden change in brightness. This was reflected by significant changes in the movement activity of the pupil, the constriction and dilation of the pupil and an increase in muscle activity. These results match those observed in earlier studies (Kum et al, 2016) and is reasonable evidence for our approach to be adequate with respect to acquisition of EMG activity, pupil size change and pupil movement activity. For the design of new stimuli that will replace the presently used stimulus, it is important to know some basic characteristic of the recorded signals. We have determined it would take 250 milliseconds for a 50% decrease in total pupil size (which was our strongest and most significant recorded signal). The approximate time it takes for the mouse to recover from a full constriction to a complete dilation can take up to 50 seconds total. This is essential information, useful in setting-up experiments and will be used as a measure for the minimum inter-trial time interval (i.e. the minimum time between two trials). The pupil constriction has the shape of a very steep exponential decay, whereas the dilation shows a linear rise. The significant drop in pupil movement activity at the onset of the stimulus may give away meaningful information about changes in attentional state. We speculate that such changes could be either a measure of stimulus strength or an indication for a difference in behavior (e.g. freezing behavior). Although some significant cross-correlation results arose from the analysis, the effect was considered negligible as anticipated. The powerful light reflex induces a strong lock on the recorded signals, which not necessarily causes a high correlation. With only 13 trials our setup was able to yield a significant change between most of the mean interval times.

After validation of the experiment setup and proposed methodology we introduced an expanding disc stimulus to the experiments, which is a well-known and strong (fear evoking) event (Yilmaz and Meister, 2013). We hypothesized a decrease of muscle activity (Steenland et al., 2012) and dilation of the pupil when fear is evoked, as well as change in relative pupil movement (Kandel, 2013). Contrary to expectations a significant increase in mean EMG activity was observed. There was constriction of the pupil after the onset of the stimulus and the pupil starts to dilate at the end of the stimulus interval. The second increase in pupil size has a slope which is less steep and we consider the effect different from the first observed peak (post-time interval). We believe that a different slope could indicate another time constant relating to another state of the animal. A strong attention-grabbing event causes fast reaction (thus a small time constant), supposed to a situation where there are no attentional demands. This is relevant information that can be used in the quantification of the signal and is thought to serve as a cue for the end of a stimulus interval. Although most mean interval times differences were not found to be significant yet, validation results and estimates from a power analysis underline the potential of the method.

Another interesting finding was a shift in the stability of the observed EMG signal in the looming disc experiments. The significant increases in overall EMG activity suggests that the mouse could be more active or aroused than before the stimulus. We believe that extensive analysis of this phenomenon could lead to a measure that allows to distinguish between active and none active behavior, this also includes the decrease in pupil movement activity and pupil size at/after the onset of the stimulus. Our reasoning is thought to be consistent with the idea of complete absence of bodily movement when a mouse freezes (Steenland et al., 2012, Steenland and Zhuo, 2008). Results indicate a small but significant rise in mean EMG activity, which is mainly due to the sudden increase at the end of the stimulus. A possible explanation for the sudden increase could be the design of the looming disc stimulus. The last component (which lasted 250 milliseconds) of the stimulus interval was a static image of the disc, from that point on no looming events would appear on the screen. The increase in EMG activity before the end of the stimulus might be explained as a reaction to this event, rather than a reaction to the stimulus. During the experiment we observed a noticeable fixation of the pupil while the stimulus was presented. The recorded pupil movement activity surely reflects this behavior by a decrease in the mean activity during the stimulus interval. Considering the recorded mean interval times to be truly a reflection of the real differences, most of the mean interval times could become statistical significance by adding less than 50 trials. This amount implies a doubling of the existing number of trials and is considered tolerable.

Mean cross-correlation between the interval times of the stimulus experiment were found to be (significantly) higher and different compared to the results from the validation experiment. These results emphasize the statement about the strong lock between the signals and the stimulus during the validation experiment and also strengthen our confidence in the conclusions we draw from the stimulus experiments. These results also reveal an obvious order of time delays between the different signals. Pupil movement seems to lead in terms of onset to an event, which is followed by the EMG activity. Constriction or dilation of the pupil can be considered to lag the most with respect to the other signals. Whether this specific order is a consequence of the used stimulus has not been investigated and could be an interesting consideration. Nevertheless, there is no complete synchronicity between any of these signals and mean correlations are still below a high correlation classification. On the other hand, the analysis of the individual trial example from the stimulus experiments show a high correlation between the different signals. Similar to the statistical results of

the interval times, we believe that there will be stronger evidence of synchronicity between signals as the experiments are progressing. Which will lead to a stronger and more sound interpretation of the present conclusions. Taken together, these results suggest that there is a detectable effect on the physical state of the mouse. We want to stress that further analysis of the presently recorded signals would be fruitful, as we are convinced that it still contains useful additional information on the state of the animal.

Besides a lack of significance between the mean interval times of the stimulus experiment, we want to elaborate on some other implications we encountered during the experiments and analysis. We think that discussing these implications is another important part of our conclusions. One of the main issues we had was to record a solid, useable heart rate signal using the pulse-oximeter. The collar-sensor was sufficient for the anesthetized recordings we did prior to the experiment, but did not yield the expected result in the awake mice. The problem appeared to be two-folded, on the one hand the collar-sensor did not fit the awake mice well and on the other hand the device was not able to produce a continuous signal (and there is no functional control over the device). Otherwise we would most likely be able to include the heart rate and breath rate signals derived, from the pulse-oximeter. Another problem arose when fixing the EMG-electrodes to the awake animal, which was deliberately not brought under anesthesia prior to the experiments. The attentive state of the animal caused a lot of movement and made it hard to get the electrodes on secure. This is an issue that needs to be addressed too, as baseline EMG values (e.g. when the animal is visually not active) are considered too high, suggesting that unwanted noise is added to the signal. It is important to solve this issue, since relevant information of the state of the animal could be lost. Besides, it will also increase the statistical relevance and usefulness of this method.

We had accounted for some issues while recording regarding to the awake state of the mouse, however we did not anticipate for the mouse's sensitiveness to audible cues (and most likely also smell). Before ultrasound recording can be used to investigate alarm cries, the setup needs to be acoustically optimized. Because of the extent of the ambient sound in the present recordings, ultrasound recordings were not considered meaningful. We want to emphasize that minimizing variations (e.g. camera distance) of the experiment setup between trials and sessions is a crucial necessity, as variations frustrate comparison of trials between sessions and lead to less significant results. Lastly, we want to share some of our thought concerning the optimization of the stimulus that will be used. As the general desired stimulus in these behavioral experiments is either a passing dot or a predator shaped object and adaptation to these object occurs rather fast (Schleidt and Shalter, 2011), it is important to include a random component of stimulus appearance.

In conclusion, our results provided very useful details about EMG, pupil size and movement recordings in an awake animal. Significant differences were observed before and after a strong light reflex stimulus, which essentially validated our experiment setup and methodology. When we consider results from the looming stimulus trials, we are confident that the follow-up experiments shall yield significant differences between the designated interval times (e.g. before during and after a stimulus is presented) within an acceptable reach of samples (trials). Additional attention to the analysis of the present data is considered a fruitful occupation, as it could valuable undiscovered information (such as heart rate and synchronized bodily movement). Thorough evaluation of the present setup identified the importance of an well designed experiment setup and eliminating any distractive cue is of great essence when working with awake mice. Overall, our findings matched our

goals regarding the expected experiment results. These findings may help us to understand behavioral research in an awake animal better and could lead to more advantageously results in future research.

## References

- Boron, W.F. & Boulpaep E.L. (2012). Medical physiology: A Cellular and Molecular Approach. *Updated 2nd edition. USA: Saunders-Elsevier.*
- Buccafusco, J.J. (2009). Methods of Behavior Analysis in Neuroscience, 2nd edition. *USA: CRC Press/Taylor & Francis.*
- Canver, M. C., Canver, A. C., Revere, K. E., Amado, D., Bennett, J., & Chung, D. C. (2014). Novel mathematical algorithm for pupillometric data analysis. *Computer Methods and Programs in Biomedicine*, 113(1), 221–225. <http://doi.org/10.1016/j.cmpb.2013.08.008>
- Chen, T.-W., Wardill, T. J., Sun, Y., Pulver, S. R., Renninger, S. L., Baohan, A., ... Kim, D. S. (2013). Ultra-sensitive fluorescent proteins for imaging neuronal activity. *Nature*, 499(7458), 295–300.
- Comoli, E., Das Neves Favaro, P., Vautrelle, N., Leriche, M., Overton, P. G., & Redgrave, P. (2012). Segregated anatomical input to sub-regions of the rodent superior colliculus associated with approach and defense. *Frontiers in Neuroanatomy*, 6(April), 9. <http://doi.org/10.3389/fnana.2012.00009>
- Cunea, A., Powner, M. B., & Jeffery, G. (2014). Death by color: Differential cone loss in the aging mouse retina. *Neurobiology of Aging*, 35(11), 2584–2591. <http://doi.org/10.1016/j.neurobiolaging.2014.05.012>
- Dana, H., Chen, T., Hu, A., Shields, B. C., Guo, C., Looger, ..... , D. S., Svoboda, K. (2014). Thy1-GCaMP6 transgenic mice for neural population imaging in vivo. *PLOS ONE*, 9(9), e108697.
- Direnberger, S., Banchi, R., Brosel, S., Seebacher, C., Laimgruber, S., Uhl, R., Felmy, F., ..... , Kunz, L. (2015). Analysis of signal processing in vestibular circuits with novel light-emitting diodes-based fluorescence microscope. *European Journal of Neuroscience*, 41, 1332–1344.
- Ebner T. J., Chen., G. (1995). Use of voltage-sensitive dyes and optical recordings in the central nervous system. *Progress in Neurobiology*, 46, 463-506.
- Grimsley, J. M. S., Sheth, S., Vallabh, N., Grimsley, C. A., Bhattal, J., Latsko, M., ... Wenstrup, J. J. (2016). Contextual Modulation of Vocal Behavior in Mouse: Newly Identified 12 kHz “Mid-Frequency” Vocalization Emitted during Restraint. *Frontiers in Behavioral Neuroscience*, 10(March), 1–14. <http://doi.org/10.3389/fnbeh.2016.00038>
- Hillman, E. M. C. (2007). Optical brain imaging in vivo: Techniques and applications from animal to man. *Journal of Biomedical Optics*, 12(5), 051402.
- Ho, D., Zhao, X., Gao, S., Hong, C., Vatner, D. E., & Vatner, S. F. (2011). Heart Rate and Electrocardiography Monitoring in Mice. *Current Protocols in Mouse Biology*, 1, 123–139.
- Ives, J. C., & Wigglesworth, J. K. (2003). Sampling rate effects on surface EMG timing and amplitude measures. *Clinical Biomechanics*, 18(6), 543–552. [http://doi.org/10.1016/S0268-0033\(03\)00089-5](http://doi.org/10.1016/S0268-0033(03)00089-5)
- Kandel, E. R., Schwartz, J. H., Jessell, T. M., Siegelbaum, S. A., Hudspeth., A. J. (2013). *Principles of neural science*, 5th edition. *USA: McGraw-Hill Medical.*
- Kum, J. E., Han, H.-B., & Choi, J. H. (2016). Pupil Size in Relation to Cortical States during Isoflurane Anesthesia. *Experimental Neurobiology*, 25(2), 1–7.

- Lanni, F., Keller, E. (2005). Microscopy and microscope optical systems. In R. Yuste & A. Konnerth (Eds.), *Imaging neuroscience* (711-765). USA: CSHL Press.
- Ledoux, J. (2013). Rethinking the emotional brain. *NIH Public Access*, 73(4), 653–676.  
<http://doi.org/10.1016/j.neuron.2012.02.004.RETHINKING>
- Liang, F., Xiong, X. R., Zingg, B., Ji, X. ying, Zhang, L. I., & Tao, H. W. (2015). Sensory Cortical Control of a Visually Induced Arrest Behavior via Corticotectal Projections. *Neuron*, 86(3), 755–767.  
<http://doi.org/10.1016/j.neuron.2015.03.048>
- Lichtman, J. W., Conchello, J. A. (2005). Fluorescence microscopy. *Nature Methods*, 2, 12.
- Lin, X., Klette, G., Klette, R., Craig, J., & Dean, S. (2003). Accurately Measuring the Size of the Pupil of the Eye. *Direct*, (November), 221–226.
- Lu, W., Tan, J., Zhang, K., & Lei, B. (2008). Computerized mouse pupil size measurement for pupillary light reflex analysis. *Computer Methods and Programs in Biomedicine*, 90(3), 202–209.  
<http://doi.org/10.1016/j.cmpb.2008.01.002>
- McAndrew, A. (2004) Introduction to Digital Image Processing with MatLab. USA: Course Technology-Thomson Learning.
- Meijer, M. K., Spruijt, B. M., van Zutphen, L. F. M., & Baumans, V. (2006). Effect of restraint and injection methods on heart rate and body temperature in mice. *Laboratory Animals*, 40(4), 382–391.  
<http://doi.org/10.1258/002367706778476370>
- Niell, C. M. (2011). Exploring the next frontier of mouse vision. *Neuron*, 72, 889-892.
- Neto, O. P., & Christou, E. a. (2010). Rectification of the EMG signal impairs the identification of oscillatory input to the muscle. *Journal of Neurophysiology*, 103(2), 1093–1103.  
<http://doi.org/10.1152/jn.00792.2009>
- Nowak, W., Żarowska, A., Szul-Pietrzak, E., & Misiuk-Hojło, M. (2014). System and measurement method for binocular pupillometry to study pupil size variability. *BioMedical Engineering OnLine*, 13(1), 1–24.  
<http://doi.org/10.1186/1475-925X-13-69>
- Paredes, R. M., Etzler, J. C., Watts, L. T., & Lechleiter, J. D. (2008). Chemical Calcium Indicators. *Methods*, 46(3), 143–151.
- Portfors, C. V. (2007). Types and functions of ultrasonic vocalizations in laboratory rats and mice. *Journal of the American Association for Laboratory Animal Science : JAALAS*, 46(1), 28–34.
- Ratzlaff, E. H., Grinvald, A. (1991). A tandem-lens epifluorescence macroscope: Hundred-fold brightness advantage for wide-field imaging. *Journal of Neuroscience Methods*, 36, 127-137.
- Reichman, J. (n.d.). Handbook of optical filters for fluorescence microscopy. Retrieved from  
[http://www.chroma.com/sites/default/files/uploads/files/HandbookofOpticalFilters\\_0.pdf](http://www.chroma.com/sites/default/files/uploads/files/HandbookofOpticalFilters_0.pdf)
- Rich, A. (1983). Shielding and Guarding. *Analog Dialogue*.
- Schleidt, W., Shalter, M. D., & Moura-Neto, H. (2011). The hawk/goose story: the classical ethological experiments of Lorenz and Tinbergen, revisited. *Journal of Comparative Psychology*, 125(2), 121–133.  
<http://doi.org/10.1037/a0022068>



- Scholle, H. C., Biedermann, F., Arnold, D., Jinnah, H. A., Grassme, R., & Schumann, N. P. (2005). A surface EMG multi-electrode technique for characterizing muscle activation patterns in mice during treadmill locomotion. *Journal of Neuroscience Methods*, 146(2), 174–182. <http://doi.org/10.1016/j.jneumeth.2005.02.006>
- Shang, C., Zijun Chen, Z., Shi, Y., Wang, Q., Liu, S., Li D., Cao, P. (2015). A parvalbumin-positive excitatory visual pathway to trigger fear responses in mice. *Science*, 348, 1472-1477.
- Simons, T. J. B. (1988). Calcium and neuronal function. *Neurosurg. Rev.*, 11, 119-129.
- Sokolowski, K., & Corbin, J. G. (2012). Wired for behaviors: from development to function of innate limbic system circuitry. *Frontiers in Molecular Neuroscience*, 5(April), 1–15. <http://doi.org/10.3389/fnmol.2012.00055>
- Steenland, H. W., Li, X.-Y., & Zhuo, M. (2012). Predicting Aversive Events and Terminating Fear in the Mouse Anterior Cingulate Cortex during Trace Fear Conditioning. *Journal of Neuroscience*, 32(3), 1082–1095. <http://doi.org/10.1523/JNEUROSCI.5566-11.2012>
- Steenland, H. W., & Zhuo, M. (2009). Neck electromyography is an effective measure of fear behavior. *Journal of Neuroscience Methods*, 177(2), 355–360. <http://doi.org/10.1016/j.jneumeth.2008.10.020>
- Suzuki, S., & be, K. (1985). Topological structural analysis of digitized binary images by border following. *Computer Vision, Graphics and Image Processing*, 30(1), 32–46. [http://doi.org/10.1016/0734-189X\(85\)90016-7](http://doi.org/10.1016/0734-189X(85)90016-7)
- Wöhr, M., & Schwarting, R. K. W. (2013). Affective communication in rodents: Ultrasonic vocalizations as a tool for research on emotion and motivation. *Cell and Tissue Research*, 354(1), 81–97. <http://doi.org/10.1007/s00441-013-1607-9>
- Wei, P., Liu, N., Zhang, Z., Liu, X., Tang, Y., He, X., ... Wang, L. (2015). Processing of visually evoked innate fear by a non-canonical thalamic pathway. *Nature Communications*, 6, 6756. <http://doi.org/10.1038/ncomms7756>
- Whelan, P. J. (2003). Electromyogram recordings from freely moving animals. *Methods*, 30(2), 127–141. [http://doi.org/10.1016/S1046-2023\(03\)00074-4](http://doi.org/10.1016/S1046-2023(03)00074-4)
- Whittaker, R. G. (2012). The fundamentals of electromyography. *Practical Neurology*, 12(3), 187–94. <http://doi.org/10.1136/practneurol-2011-000198>
- Yilmaz, M., & Meister, M. (2013). Rapid innate defensive responses of mice to looming visual stimuli. *Current Biology*, 23(20), 2011–2015. <http://doi.org/10.1016/j.cub.2013.08.015>

## Appendix

### I – Acquisition and analyzing scripts.

All used acquisition and analyzing scripts were custom made to fit the specific needs of the research aim and the used (acquisition-) hardware. A total of 23 MatLab scripts were written for the acquisition parts besides 20+ additional scripts for the analysis. The video acquisition software was developed in C++ to fully use all the capabilities of the used hardware. All scripts can be viewed and downloaded either from <https://github.com/heimel/InVivoTools/tree/master/Physiology> (InVivo Toolbox Github repository) or from <https://github.com/Lansbergen>. These repositories also include the configuration-files that contain the parameters used in various analysis and acquisition operations.

### II – Detailed statistical test results.

The results sections refers to detailed statistical test results, which we present in the tables below. Tables A-1, A-2 and A-3 are test results from the validation experiment and table A-4 and A-5 are the test results from the looming disc stimulus.

#### **Statistical results section 1 (validation) :**

P-value	EMG	Pupil Size	Pupil Movement
Pre-time	5.4896e-05	7.5639e-13	5.3334e-07
Post-time	7.4179e-06	7.5639e-13	4.5623e-05
Stimulus	2.0019e-05	7.5639e-13	3.9412e-06

Table A1 – Kolmogorov-Smirnov goodness-of-fit test results validation data (n=13). Test if data is normally distributed, against alternative that the data is not normally distributed.

P-value	EMG	Pupil Size	Pupil Movement
Pre-time vs. Post-time	0.0061035	0.00048828	0.21631
Pre-time vs. Stimulus	0.0080566	0.00024414	0.0012207
Post-time vs. Stimulus	0.19092	0.001709	0.37573

Table A2 – Wilcoxon signed rank test results validation data (n=13). Test the hypothesis of zero median for the difference between the interval times.

	EMG	Pupil Size	Pupil Movement
Pre-time vs. Post-time	0	0	>25
Pre-time vs. Stimulus	0	0	0
Post-time vs. Stimulus	15	0	20

Table A3 – Power analysis validation data: the number of additional trials needed before a 80% of that number is statistical significant ( $p < 0.05$ ), results >25 were rejected.

**Statistical results section 2b (looming disc stimulus) :**

P-value	EMG	Pupil Size	Pupil Movement
Pre-time vs. Post-time	6.8915e-17	4.3341e-41	9.7565e-16
Pre-time vs. Stimulus	3.2484e-17	4.3341e-41	4.0934e-17
Post-time vs. Stimulus	2.041e-17	4.3341e-41	9.2274e-15

Table A4 – Wilcoxon signed rank test results looming stimulus data (n=45). Test the hypothesis of zero median for the difference between the interval times.

P-value	EMG	Pupil Size	Pupil Movement
Pre-time	0.029791	0.92356	0.31782
Post-time	0.0025326	0.12065	0.3345
Stimulus	0.71373	0.22497	0.16331

Table A5 – Kolmogorov-Smirnov goodness-of-fit test results looming stimulus data (n=45). Test if data is normally distributed, against alternative that the data is not normally distributed.